UCID-17038

Lawrence Livermore Laboratory

PRESENT STATUS OF MIRROR STABILITY THEORY

D. E. Baldwin, H. L. Berk, J. A. Byers, R. H. Cohen, T. A. Cutler, N. Maron, L. D. Pearlstein, M. E. Rensink, T. D. Rognlien, J. J. Stewart, D. C. Watson, and M. J. Gerver*

February 11, 1976

*Electronic Research Laboratory, UC Berkeley

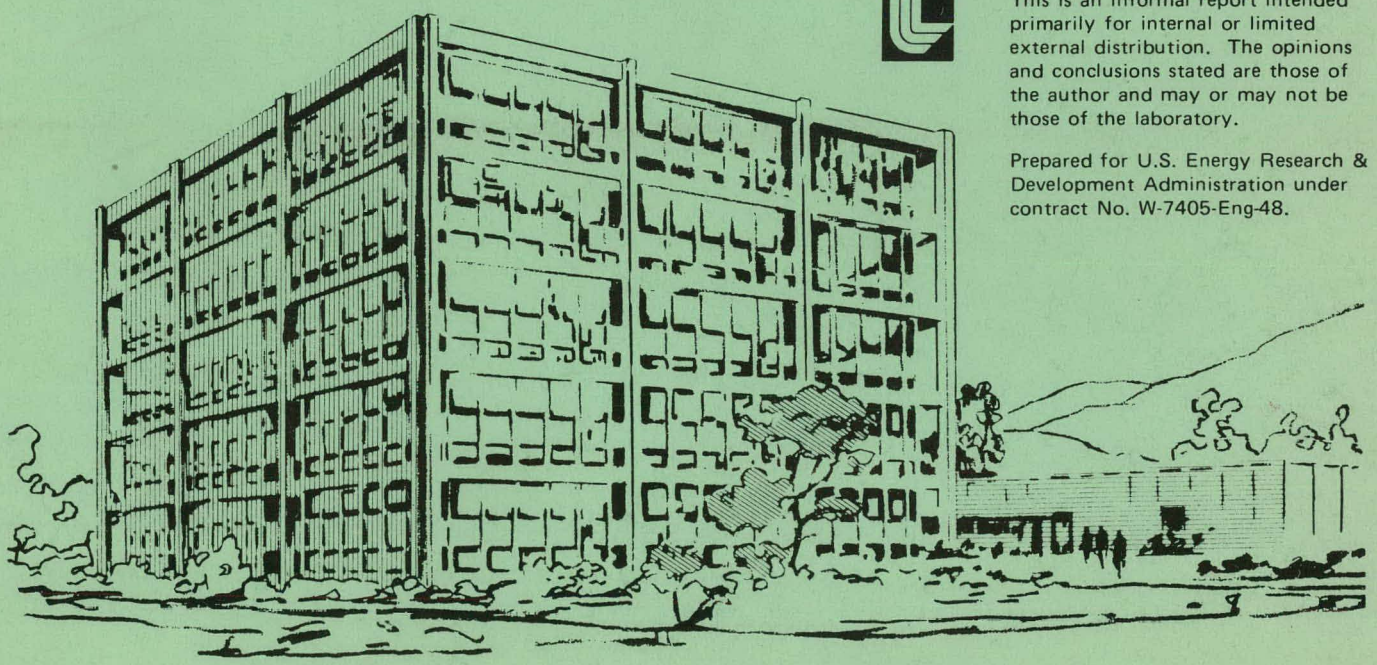

Prepared for U.S. Energy Research & Development Administration under contract No. W-7405-Eng-48.

DISCLAIMER

CONTENTS

PRESENT STATUS OF MIRROR STABILITY THEORY

ABSTRACT

A status report of microinstability as it applies to 2XIIB and MX theory for mirror machines is presented. It is shown that quasilinear computations reproduce many of the parameters observed in the 2XIIB experiment. In regard to large mirror machines, there are presented detailed calculations of the linear theory of the drift cyclotron loss-cone mode, with inhomogeneous geometry and nonlinear diffusive effects. Further, the stability of a mirror machine to the Alfvén ion-cyclotron instability is assessed, and the Baldwin-Callen diffusion is estimated for a spatially varying plasma.

INTRODUCTION

Theoretical support for the mirror program can be divided into three related parts:

- Understanding and describing existing experiments,
- Predicting stable parameters for larger experiments, and
- Determining equilibrium and loss characteristics of both classes of experiments (with the assumption that they behave stably).

The third-named effort is of initial importance in designing any large-scale, high-β experiment and in assessing the economic viability of a mirror reactor. We have been operating a time-dependent, two-velocity-dimensional, Fokker-Planck code to which we are now adding the effects of axial-bounce average and velocity-space transport due to fluctuating fields. Two codes have been developed to generate three-dimensional, finite-β,

guiding-center equilibria. An axisymmetric, electromagnetic code investigates the related questions of the β-limits due to the mirror mode, the possibility of field reversal, and axisymmetric instability thresholds. The results of these efforts will be described at a later date.

In what follows, we first describe in detail the results of a quasilinear modeling of 2XIIB in which it was assumed that the distribution function was driven to marginal stability, as would be the case for a plasma dominated by the drift cyclotron loss-cone (DCLC) mode. The corroboration of theory with experiment is impressive. Next, the results of this theory are extrapolated and combined with the results of linear theory for those other modes thought to be significant. The combination provides a stability-parameter picture of MX and a mirror reactor.

RESULTS OF QUASILINEAR SIMULATION OF THE 2XIIB EXPERIMENT

Here, we shall describe some of the results of our quasilinear simulation code as it applies to the 2XIIB experiment. The code itself is described in Appendix A. The basic equations used in the simulation to describe the distribution function F and the electron temperature T_e are given by Eqs. (A1) and (A11) in that Appendix. For the growth rate [in Eq. (A5)], we use $\sigma_k = 1$ and $m = 2$. We have chosen this "ad hoc" form for the growth rate because in 2XIIB we expect that the distribution evolves to a state of marginal stability that depends just on the shape of the distribution function rather than on the detailed dynamics of the modes.[1,2] We have found that our results are insensitive to σ_k or m. The important point is that the diffusion coefficient grows to a level that maintains marginal stability.

In the results we shall present here, the effect of $T_{\parallel}$ is neglected. The one-dimensional transport equation used here can only crudely take $T_{\parallel}$ into account, and the additions to the HYBRID II code currently being developed by T. Rognlien (see Appendix B) will treat the effect of $T_{\parallel}$ more accurately.

First of all, we shall discuss results neglecting charge exchange from background gas and keeping the stream current constant. We impose a beam current with a total buildup time τ_B, where $\tau_B^{-1} = \tau_{CHX}^{-1} + \tau_{ion}^{-1}$ and $\tau_{ion} = 1.69$ ms is the ionization buildup time, and $\tau_{CHX} = 0.56$ ms is the charge-exchange replacement time. A stream current, $J_{STRM} \equiv \int_0^\infty dv_\perp^2 \, S_{STRM}(v_\perp^2) = 2.15 \times 10^{17}$ particles/cm^3·s, is imposed. The energy spectrum of the beam is centered at 18, 9, and 6 keV with a relative weight of 6:3:1, respectively. The initial plasma is taken as a Maxwellian at 2 keV and a density of 3×10^{13} cm^{-3}.

In Fig. 1, we see the normalized distribution early in time before turbulent diffusion modifies the distribution. We see the structure of the three beam components plus the phase-space hole that has developed in the initial Maxwellian distribution due to the particles that we lost in a transit time.

Eventually, this distribution reaches a steady state and diffuses into the steady-state shape shown in Fig. 1. The turbulence is large enough to spread the input beam width considerably although the shape of the distribution function is influenced by an input beam.

In Figs. 2(a) through 2(d), we show the time evolution for $0 < t < 2$ ms of the (a) density; (b) ion and electron temperature; (c) $n\tau$ of the particles, energy, and drag; and (d) wave energy arising from turbulence. It is clear from Fig. 2 that a steady state is achieved with a stream input.

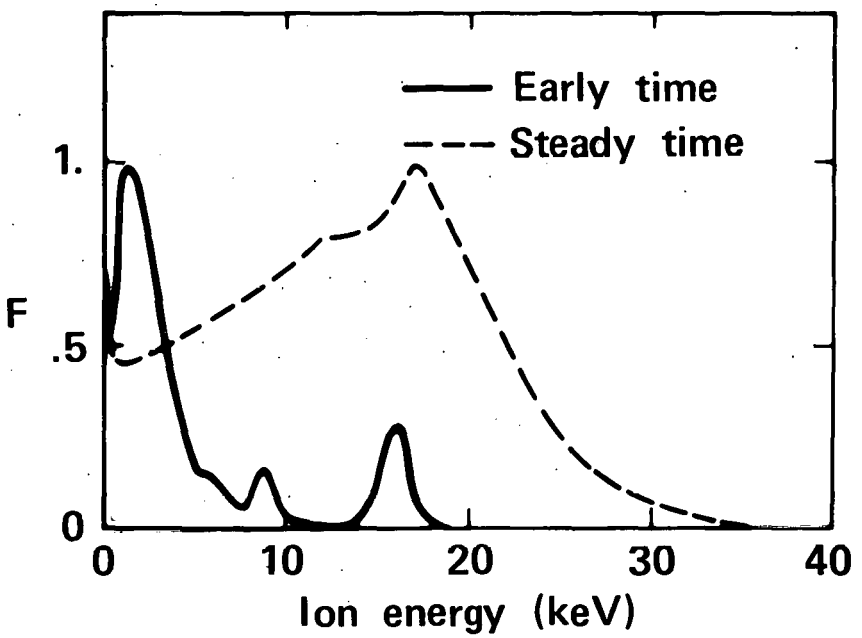

Fig. 1. Early-time and steady-state ion distribution when plasma stream is present and charge exchange with background gas absent. Initial parameters are J_{ST} (stream current) = 2.15 X 10^{17} particles/cm^3•s, ionization time τ_{ion} = 1.69 ms, and charge-exchange replacement time τ_{CHX} = 0.56 ms.

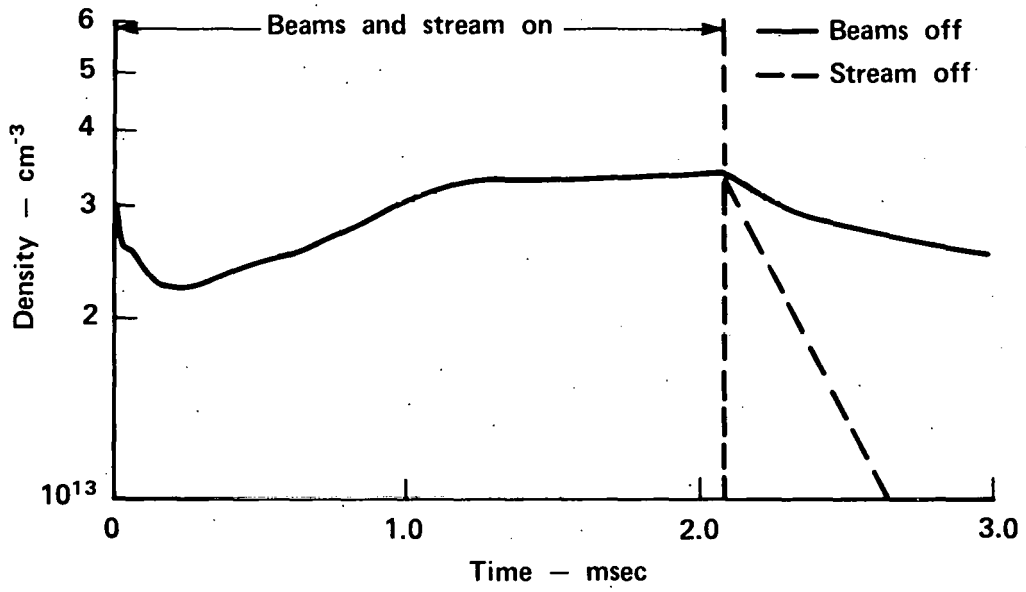

(a) plasma density

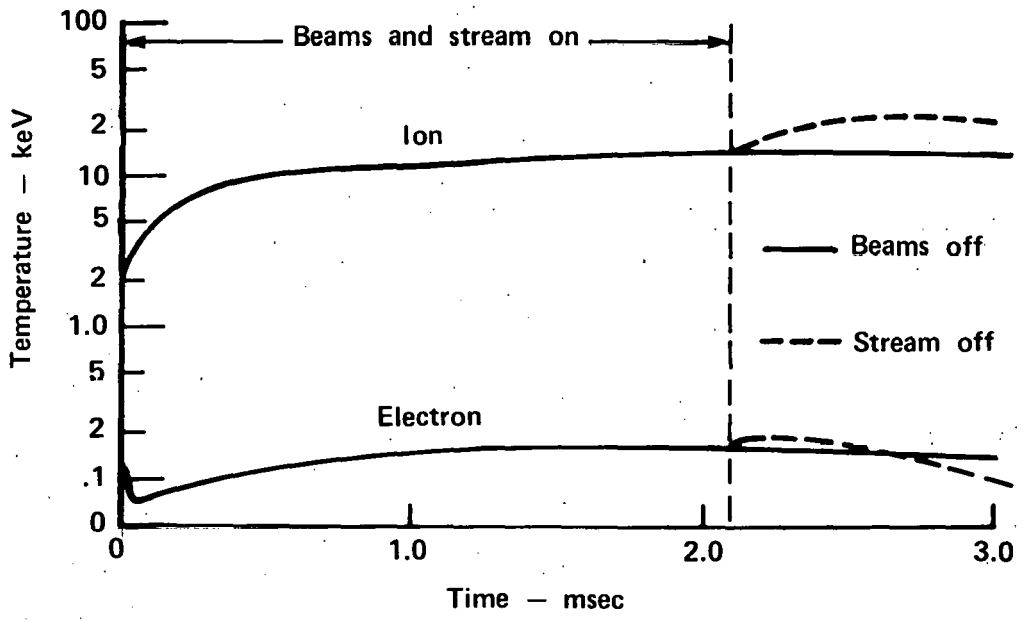

(b) electron and ion temperatures

Fig. 2. Time development of plasma parameters vs time (same conditions as for Fig. 1).

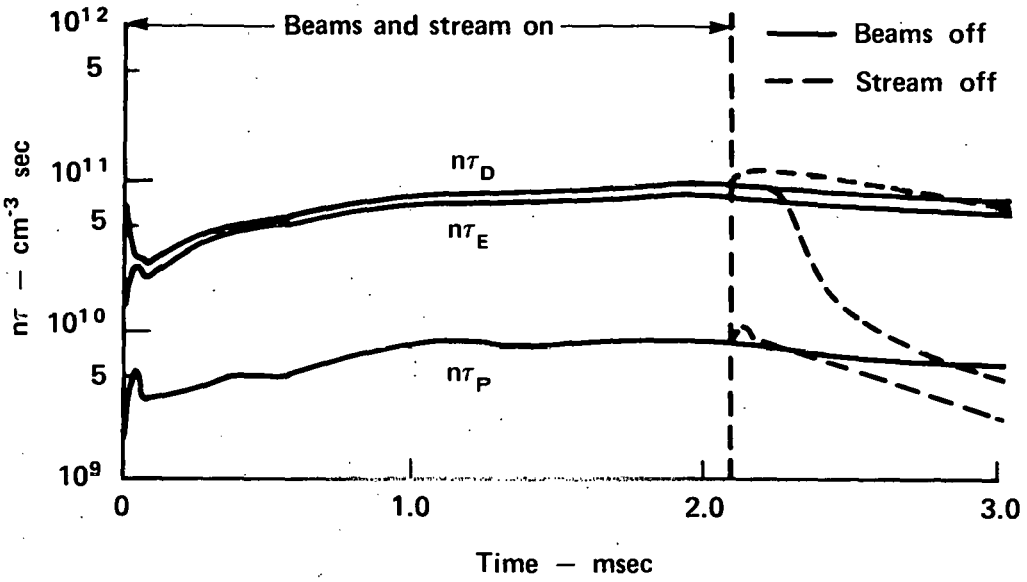

(c) $n\tau$ for particles, energy and drag

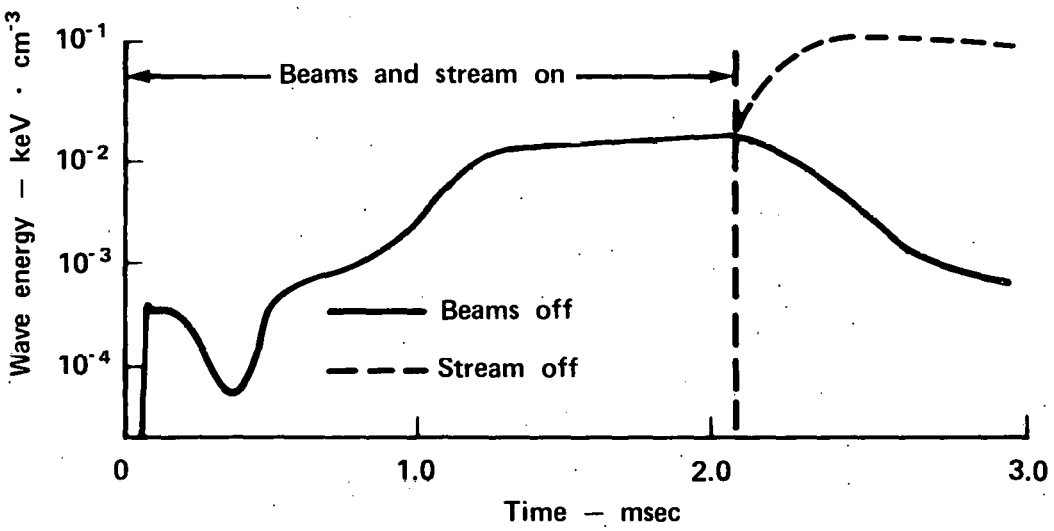

(d) wave energy

Fig. 2. (continued)

The plasma parameters achieved in this steady state correlate closely with experiment in 2XIIB, as can be seen in the comparison in Table 1.

The scaling laws of the steady state achieved can be understood as follows. In steady state, we have that the power into electrons is equal to their power lost out the ends, or

$$n\nu_{DRAG}T_i = \eta \frac{\partial n_L}{\partial t} T_e \ . \tag{1}$$

[See Eq. (A11) for definitions.] Secondly, in steady state the density-loss rate $\partial n_L/\partial t$ is equal to the input rate so that

$$\frac{\partial n_L}{\partial t} = n \int_0^\infty dv_\perp^2 \, S_{BEAM}(v_\perp^2) + J_{STRM} \ . \tag{2}$$

Now, $\partial n_L/\partial t$ can also be estimated from quasilinear theory to be the fraction of the plasma in the loss cone times the transit rate $\nu_{TRANSIT} \approx 0.5(q\Phi/M)^{1/2}/L_p$ of unconfined particles. Typically, $q\Phi/T_e \approx 3$. At marginal stability, the unconfined plasma density n_u is

$$n_u = n\lambda q\Phi/T_i \approx 3n\lambda T_e/T_i \ , \tag{3}$$

where λ is a constant of order 0.5. Now, using $\partial n_L/\partial t = \nu_{TRANSIT} n_u$, Eq. (1) becomes

$$n\nu_{DRAG}T_i = \frac{3\sqrt{3}}{2} \eta n\lambda \left(\frac{T_e}{M}\right)^{1/2} \frac{T_e^2}{T_i} \ . \tag{4}$$

From Eq. (4), we obtain T_e as a function of T_i and particle density. Expressing T_e and T_i in units of keV and using $\nu_{DRAG}^{-1} = n/(1.4 \times 10^{12} \, T_e^{3/2})$, we find

$$T_e = 8.8 \times 10^{-6} \left(\frac{nL_p T_i^2}{\lambda\eta}\right)^{1/4} \ . \tag{5}$$

Table 1. Correlation of quasilinear, steady-state calculation with stabilizing stream with observed experimental parameters.

	Theory	Experiment
$n\tau$ ($cm^{-3} \cdot s$)	8.7×10^{10}	5.7×10^{10}
Density (cm^{-1})	4×10^{13}	3×10^{13}
Ion energy (keV)	13	13
Electron temperature (eV)	170	140

If the stream current greatly exceeds the beam current, we can substitute Eq. (2), neglecting the beam term, into Eq. (5) and obtain

$$n = 0.6\, J_{STRM}^{8/11} L_p^{5/11} T_i^{2/11} \eta^{3/11} / \lambda^{5/11} , \tag{6}$$

$$T_e = 7 \times 10^{-6}\, J_{ST}^{2/11} L_p^{4/11} T_i^{6/11} / (\eta^{2/11} \lambda^{4/11}) .$$

This scaling law correlates with observed simulation results when various input parameters are varied. Note the steady-state density and electron temperature that are achieved are independent of beam input, but dependent on the stream input.

Another important point is that the ion-energy containment time is basically the electron-drag time. This can be seen by noting that the ion power-density drain by direct transit loss is less than the power-density drain to electrons. The transit power drain, P_L, is

$$P_L \doteq 0.5 q \Phi\, \partial n_L / \partial t . \tag{7}$$

Comparing this expression with Eq. (1), we see that P_L is less than the electron-drag drain $n \nu_{DRAG} T_i$ if $\eta > 1.5$.

The simulation in Fig. 2 was continued for $t > 2$ ms by introducing various options of turning off either the stream or the beam. When the stream is turned off, buildup no longer continues, and the density falls. In general, it is found that the turbulence generated without the stream prevents plasma buildup. Observe that the ion temperature increases dramatically without stream. In fact, the ion distribution runs away to high energy until the ions are lost on the upper energy boundary of the calculation. The continual hardening of the ion distribution in our model can be qualitatively understood by noting that when an ion is lost, it leaves with an energy comparable to the ambipolar potential, which is less than the mean ion energy. Hence, this effect tends to increase the ion energy. Only

the electron drag can stop the ion runaway, but as the density is falling, the electron-drag rate continually decreases while the ion-diffusion term, which is independent of density, continues to cause ion runaway.

When the beam is turned off and the stream is on, one observes a decrease of more than a decade in the turbulent wave energy. In part, this is due to lack of charge exchange off the beam. The diffusion term, which drives the distribution to marginal stability, need not be as large because it no longer has to compensate for charge-exchange loss to maintain the shape of the distribution function at marginal stability. Further, the electron temperature is decreasing, and hence the unconfined region in the distribution becomes smaller. Hence, the diffusion coefficient needed to achieve marginal stability becomes less. When the beam and stream are both turned off, the results are quite similar to when the stream is turned off.

When charge exchange on the background gas is included in our equations, we can appreciably alter the response of the system. Apparently, the reduced density due to charge exchange reduces the power input into electrons and hence cools the electrons. In Fig. 3, we plot the electron and ion temperatures and density as a function of a constant charge-exchange time for otherwise similar conditions as used for Figs. 1 and 2.

In addition, we find that in the absence of stream the ion-runaway rate is greatly reduced. We can eliminate the ion-runaway rate completely by assuming that high-energy particles in 2X are more likely to charge exchange with low-energy neutrals because their orbits carry them closer to the edge of the plasma where the neutral density is higher. To mock-up this effect, we have multiplied the charge-exchange rate by a factor exp (E/E_{CHX}), where we have chosen E_{CHX} = 30 keV in the calculation we report below.

In order to compare our simulation in detail with an experimental run, we need to include the fact that both the charge-exchange rate and stream are

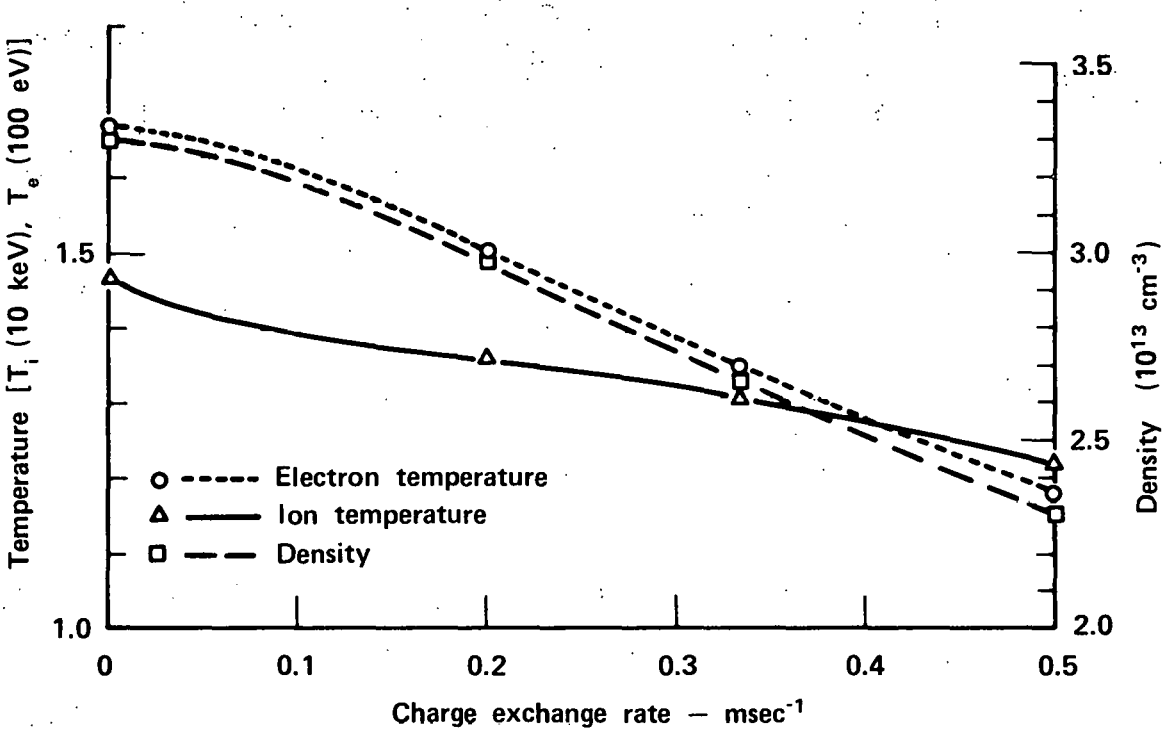

Fig. 3. Effect of constant charge-exchange rate from background gas on steady-state electron and ion temperatures and plasma density. Same beam and stream conditions as in Fig. 1.

continuously time dependent. In the experiment when the beam current is turned on, there is a source of gas that enters the plasma chamber that is roughly proportional to the beam current and beam-duration time. Consequently, in Eq. (A1), we have allowed the charge-exchange rate ν_{CHX} to increase linearly with time until the beams are shut off, and then remain constant. From the observed charge-exchange flux after the beam is turned off, one can estimate the final charge-exchange rate.

Experimentally, Molvik has been able to infer the stream current by using an end-loss analyzer at one of the ends of the mirror machine. On the particular run we have analyzed, we find that the end-loss current increases a factor of four during the time the stream is on. We have approximated the time dependence of the stream with the function

$$S_{STRM} = \begin{cases} S_{STO}\left[1 + \beta \dfrac{\left(e^{t/\tau_1} - 1\right)}{e - 1}\right] & t < \tau_1 \\ S_{STO}\,[1 + \beta]\, e^{-t/\tau_2} & t > \tau_1 \end{cases}$$

where $\beta = 3$, $\tau_1 = 1.2$ ms, and $\tau_2 = 0.25$ ms. For S_{STO}, we use 6.8×10^{16} particles/cm^3·s. The rise-time parameters of the input beam are $\tau_{ion} = 0.60$ ms and $\tau_{CHX} = 0.20$ ms. The beams are injected at 14, 7, and 4.67 keV at a relative weight of 5:4:1.

In the actual experiment, 300 A of neutral beam is injected, and an end current at the computer t = 0 time of about 10 A is inferred (however, there is an uncertainty in the absolute calibration of the end current). If the end current leaves at an equal rate from both sides of the machine and we take a plasma volume of 4.5 ℓ, we infer a stream density of 2.8×10^{16} particles/cm^3·s. However, considerable calibration and geometrical uncertainty exist in the experimental numbers, and the computer

simulation parameters of S_{STO} and S_{BEAM} were chosen to best fit the experimental density rise-time characteristics. Actually, the calibration of simulation parameters to experiment was done on one experimental run, and this synchronized quite well with several other detailed experimental-simulation comparisons.

In Fig. 4, we compare the time variation of several physical parameters in the computer simulation and in an experimental run. We see that the density and ion temperature correlate quite closely in the two runs. The electron temperature was measured in the experiment at only one point in time, and it is in close agreement with the computer simulation.

In both the computer simulation and the experiment, there is a break in the rise time at 0.4 ms. The experiment was characterized by turbulent "bursting"[3] between 0.4 and 0.7 ms. In the plasma simulation, the noise is saturated in the same time interval. An interpretation that appears consistent is that at 0.4 ms, the plasma density achieves the steady-state density determined by the stream. However, the stream is increasing with time, and hence the density increases in accordance to the increase in the stream-input rate.

The comparison of the plasma-decay rate in the absence of beam is very close in both the experiment and the simulation. After the stream is turned off, it takes, in the simulation, about 200 μs for the turbulent noise to increase to a high-enough level to increase the decay rate. The actual experiment takes 150-μs longer before additional noise and more rapid decay are observed. The increase in the noise causes the ion temperature to increase in both experiment and simulation, although the temperature increase is more pronounced in the simulation.

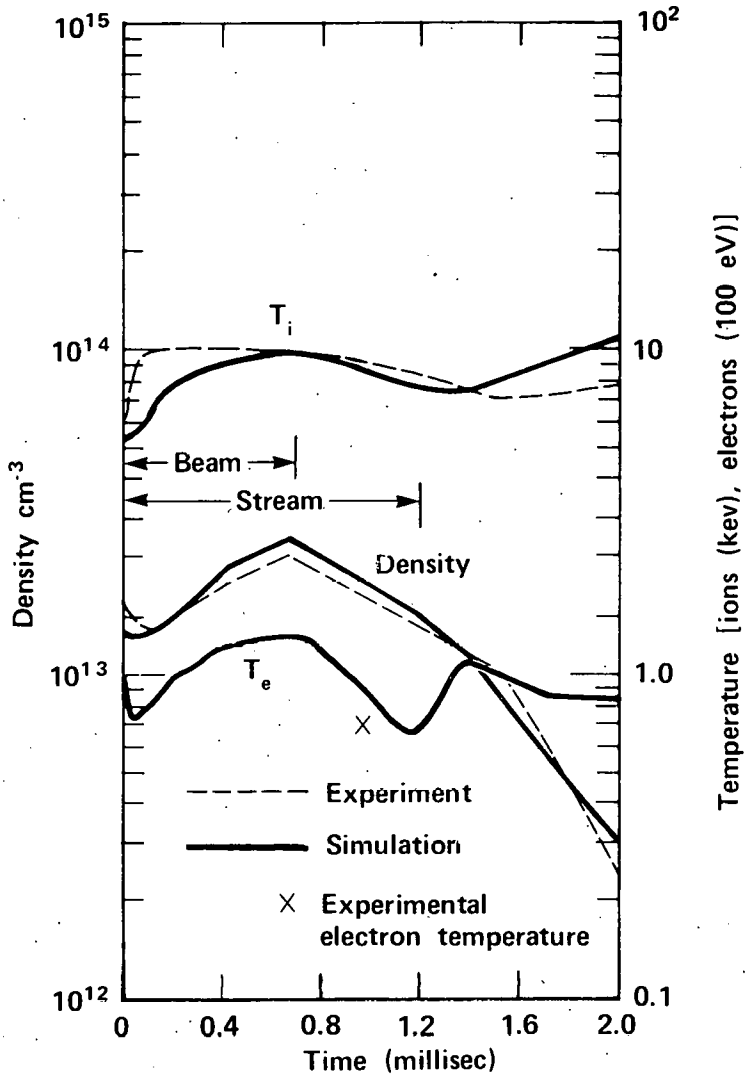

Fig. 4. Comparison of ion and electron temperature and plasma density between quasilinear computation and experiment. Charge-exchange rate with background gas and stream current vary in accordance with experimental observation. Initial beam-buildup rate synchronized with experimental observation.

In summary, we find that a relatively simple, one-dimensional, quasilinear model produces very good correlation with experiment in predicting density and electron and ion temperatures. We are trying to improve the code by including the stabilizing effect of larger radial-scale lengths on the unstable modes and to include the effect of $T_{\parallel}$ that arises from ion-ion pitch-angle scattering and the finite-beta mirror condition.

CRITERIA FOR STABILITY

The 2XIIB phenomena described in the previous section have been ascribed to the drift cyclotron loss-cone mode (DCLC). Experimental incidence for this mode identification is given in Ref. 4.

Many of the results described in the preceding section can be scaled to machines of larger size, and the corroboration with current experiments lends confidence to this extrapolation. In addition, there are other important phenomena, not as dominant as the DCLC mode in 2XIIB, which have been less intensively studied and have been only incompletely or inconclusively corroborated by experiment. The implication of these modes for mirror confinement is now coming under more careful scrutiny. Just as is the case with the DCLC mode, the stability boundaries of these modes, as confirmed by experiment, will determine the gross features of a mirror reactor. In the next several sections, the present status of each phenomenon is described.

Alfvén Ion-Cyclotron Mode

In addition to inverted populations in velocity space that can generate instabilities in the ion-cyclotron frequency range, a mirror-confined plasma must maintain anisotropic ion-velocity distributions. This departure from

thermodynamic equilibrium suggests the presence of unstable modes. The mirror mode is one such case which puts a limit on $\beta_\perp$ as a function of the temperature anisotropy, $T_\parallel/T_\perp$ (or equivalently R, the mirror ratio). Such constraints are an important consideration for buildup and for the achievable steady state and are combined with Fokker-Planck studies to determine limiting betas.

Recently it was pointed out[5] that a left-hand, circularly polarized Alfvén wave destabilized by anisotropy might put a more stringent $\beta_\perp$ limit on mirror machines. Although these waves can be convective, prior calculations of this mode[6] ignored finite-geometry effects and produced growth rates and frequencies for real $k_\parallel$, wavenumber parallel to $\underset{\sim}{B}$.

We are presently ascertaining the influence of this mode on mirror machines of finite extent. Specifically, we determine:

- The boundary between absolute and convective instability $\left(\frac{d\omega}{dk_\parallel} = \mathrm{Im}\omega = 0\right)$ and the influence of finite geometry on this boundary by solving the phase integral[7]

$$\int_{-s_T}^{s_T} k_\parallel ds = (2n + 1)\pi \ , \quad \left(\frac{d\omega}{dk_\parallel}\right)_{s_T} = 0 \ ,$$

  where s is the distance along a field line, and ω is the complex eigenfrequency.
- The convective growth of a wave pocket in the convectively unstable region.
- The modifications due to radial variation that are significant for plasmas with a few Larmor diameters across the plasma.

Before presenting results, we review the properties of the mode. The dispersion relation is obtained by solving the perpendicular components of Maxwell's equation ($\underset{\sim}{E} \cdot \underset{\sim}{B} = 0$ due to the mobility of electrons along the

field line). In the limit $k_\perp = 0$ ($k_\perp$ is the perpendicular wavenumber), the solution reduces to a left-hand, circularly polarized Alfvén wave satisfying the dispersion relation

$$k_\parallel^2 V_a^2 = \frac{\omega^2 \omega_{ci}}{\omega_{ci} - \omega} + \int d^3v \left[\frac{\omega_{ci}}{\omega_{ci} - \omega} f(v) + \frac{\partial}{\partial v_\parallel^2} v_\perp^2 f(v) \right] \frac{k_\parallel v_\parallel}{\omega - \omega_{ci} - k_\parallel v_\parallel} ,$$

where V_a is the Alfvén velocity, ω_{ci} the ion-cylcotron frequency, and f the distribution function normalized to unity. In the asymptotic limit ($k_\parallel v_\parallel << |\omega - \omega_{ci}|$), one then obtains

$$\omega \approx \omega_{ci} \left[1 + i \sqrt{\frac{\beta_\perp}{2} \left(1 - \frac{T_\parallel}{T_\perp} \right)} \right] ,$$

which for high beta and strong anisotropy produces a strong growth rate that was the cause for concern. For weak anisotropy, growth rates are proportional to $\exp \left[-\beta_\perp^{-2} (T_\perp / T_\parallel - 1)^{-2} \right]$; i.e., they are exponentially small. To ascertain the significance of such weakly growing waves requires a study of the convective growth length, which becomes very small as the mode becomes absolute.

To evaluate stability boundaries, we consider two specific distributions, a bi-Maxwellian (A),

$$f \sim e^{-\alpha_\perp v_\perp^2} e^{-\alpha_\parallel v_\parallel^2} , \tag{8}$$

and a Holdren-type distribtuion (B),

$$f \sim v^{2N} e^{-\alpha v^2} g(v_\perp^2 / v^2). \tag{9}$$

Note that in general, distributions should vanish for $v \to 0$; hence $N > 0$. However, the present analysis is limited to $N = 0$ to simplify the algebra; we are studying the effects of $N \neq 0$. Our preliminary results are depicted in Fig. 5 and Table 2. In Fig. 1, we compare the mirror-mode boundary for a

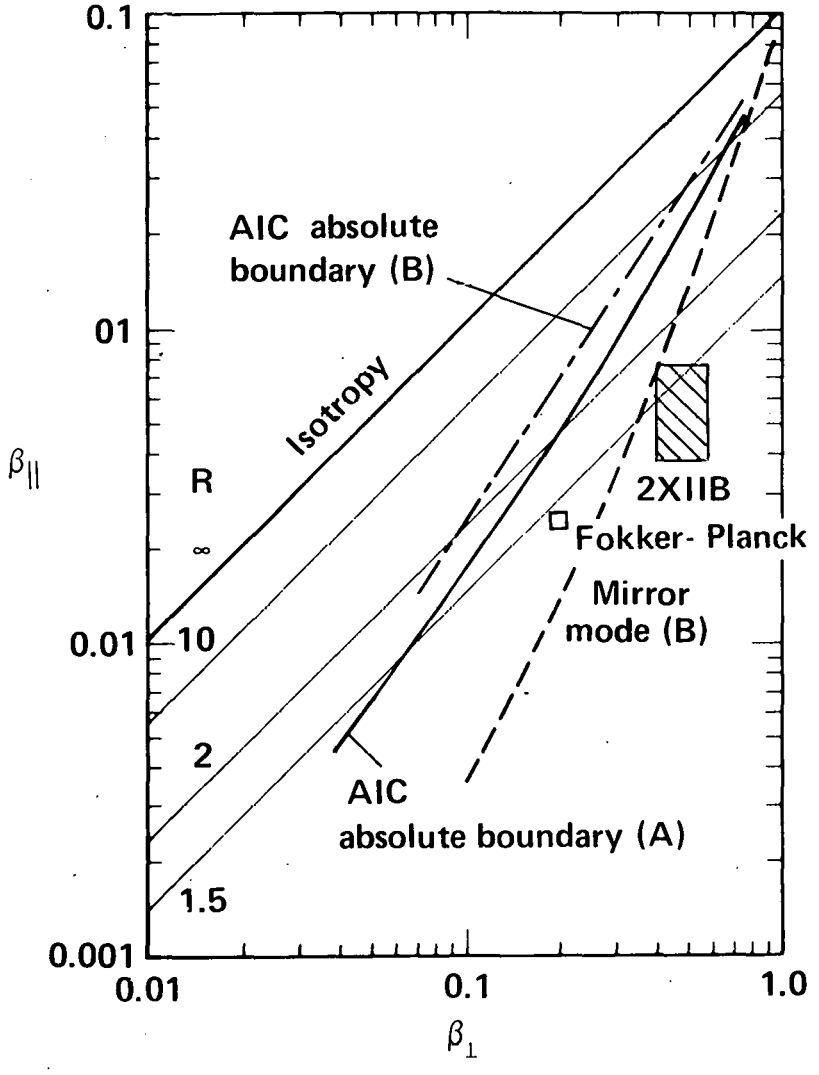

Fig. 5. Stability boundary to absolute Alfven ion cyclotron (AIC) mode.

Table 2. Plasma parameter comparison for the Alfvén ion cyclotron (AIC) mode.

	2XIIB Parameters	MX Parameters
E_{ions}	13 KeV	50 KeV
B_{vacuum}	7 kg	20 kg
$\beta_{\perp}$	0.5	0.5
ρ_{ions}	4.2 cm	3.2 cm
$R^{\text{full length}}_{\text{with plasma}}$	2.8	2.8
$R^{\text{plasma length}}_{\text{with plasma}}$	1.64	1.6
$\ell^{\text{center to edge}}_{\text{plasma}}$	30 cm	80 cm
$\ell^{\text{center to edge}}_{\text{plasma}}$	$\equiv 7.1\ \rho_{i\parallel}$	$\equiv 25\ \rho_{i\perp}$
$L_{growth}/\rho_i = 7.5$, $\lambda_1/\rho_i = 14.4$	at Alfven ion cyclotron mode boundary	
$L_{growth}/\rho_i = 4.4$, $\lambda_1/\rho_i = 8.8$	at mirror mode boundary	

Holdren normal-mode distribution to the convective absolute boundary for the Alfvén instability computed for distributions A and B. For these distributions, we see that in the infinite-medium limit the maximum β attainable is below the mirror-mode limit.

Present estimates show that for 2XIIB the modifications due to the small radius (in units of Larmor radii) are unimportant.

The effect of the modifications due to length are unclear in 2XIIB. For the experimental configuration at 13 keV (see Table 2), it is seen that the wavelength of the mode is equal to the length of the plasma, thereby casting doubt on the reliability of the calculation. Further, the WKB correction to the growth rate is approximately half that of the infinite-medium answer, again suggesting a strong distortion. These results all suggest the need for a complete treatment of the spatial normal-mode problem. On the other hand, the plasma parameters obtained from a Fokker-Planck computation of MX buildup suggest that the infinite-medium theory should be more accurate here. However, it is important to realize that the mode is sensitive to the detailed distribution function, and further improvements in our calculations await studies with more realistic distributions to be obtained from extended two-dimensional Fokker-Planck calculations incorporating turbulent diffusion. It should be pointed out that there is a discrepancy between the low beta limit predicted by analytic theory and that observed in the experiment and in the particle simulation code (SUPERLAYER).

Stability Boundaries for the DCLC and Negative-Energy Modes

The stability boundary for the DCLC mode and the negative-energy wave for various warm-plasma fractions and hole size have been determined. Prior

calculations (Appendix C) have determined this boundary by setting the local dispersion relation evaluated at the midplane equal to zero: $I(\omega, k_\perp, s=0, \text{parameters}) = 0$. The appropriate normal-mode analysis[8] shows that the pertinent dispersion relation (L is the plasma length) is

$$\int_0^L ds k_\perp^2 \, I(\omega, k_\perp, s, \text{parameters}) = 0.$$

In addition to this refinement, we have included the influence of the quasilinear turbulent-diffusion coefficient on the particle orbits (orbit diffusion) in the dispersion relation through the addition

$$\omega - n\omega_{ci} \rightarrow \omega - n\omega_c + ik^2 D \left(\frac{\omega}{k}\right)$$

for the ions and similarly for the electrons so that

$$I = \frac{\omega_{pe}^2}{\omega_{ce}^2} + 1 + \frac{\omega_{pi}^2}{\omega_{ci}^2}\left[- \frac{\omega_{ci}}{k_\perp R_p} \frac{1 + \beta_\perp/2}{\omega + ik_\perp^2 D_e} + \sum \frac{F_n(k_\perp a_i)\omega}{\omega - n\omega_{ci} + ik_\perp^2 D} \right].$$

The results of these surveys are depicted in Figs. 6 and 7. In Fig. 6, we show the fraction of warm plasma required to stabilize a 2XIIB- or MX-size plasma as a function of radius for $\beta_\perp = 0.3$ and $\beta_\perp = 0.5$ for a range of $(v_H/v_h)^2$. Note that v_H is the average perpendicular velocity of the confined plasma and that v_h (the hole velocity) is the mean velocity of the missing part of the loss-cone distribution. From the graph, we see that there is a reduction in required warm-plasma fraction of about a factor 6 in going from 2XIIB to the high-beta operation in MX. From the predicted electron temperature, also plotted on Fig. 6, there is a 10-fold increase in $n\tau_E$. Fig. 7 shows the relation between stable radius and inverse density for a mean ion energy of 50 keV for no warm plasma and for fractions of stabilizing warm plasma equal to 10^{-4} and 10^{-2}. For a level of 10^{-4}, the electron-temperature model shown in Fig. 6 gives $T_e = 3.7$ keV; whereas for 10^{-2}, $T_e = 0.7$ keV, as compared with the classical value of 5 keV.

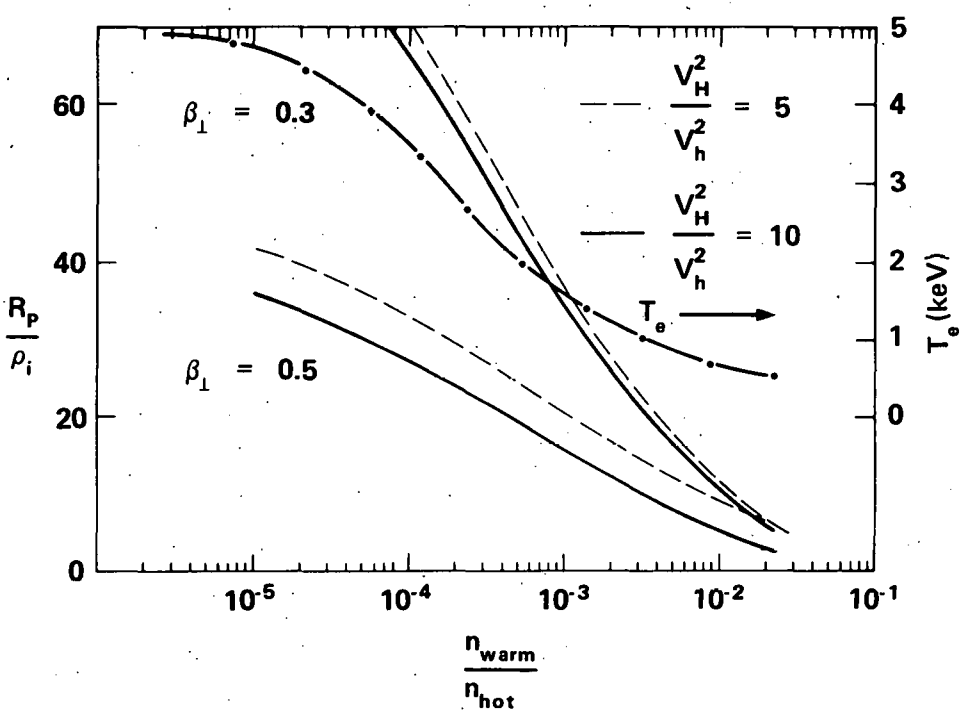

Fig. 6. Minimum plasma radius and predicted electron temperature vs the fraction of a warm plasma.

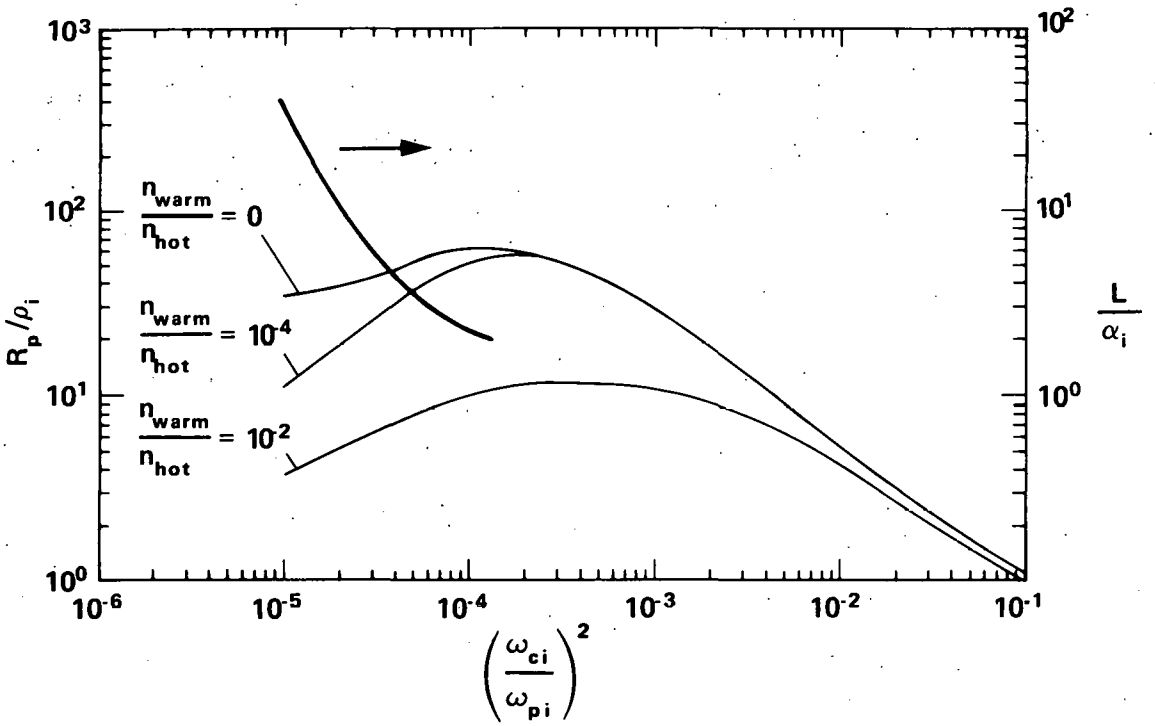

Fig. 7. Stable radius and maximum axial scale for stable negative energy wave as a function of $(\omega_{ci}/\omega_{pi})^2$ for various fractions of warm plasma.

The marked reduction in the size of the stable radius at high density is due to two cooperative effects. One is the stabilizing influence of beta described elsewhere,[9] and the other is that orbit diffusion reduces the magnitude of the perpendicular wavenumber, which makes the beta term that much more effective.

In Fig. 7 we also show the maximum axial magnetic scale length consistent with stability to the flute-like, negative-energy wave. We are determining the maximum scale-length restrictions from the higher axial normal modes (q_s = 1, 2, ...).

High-Frequency Convective Loss-Cone Mode

The axial length of a mirror machine is limited by the Rosenbluth-Post convective mode.[10] This mode amplifies while propagating almost parallel to $\underset{\sim}{B}$ with $\omega \sim \omega_{pi}$, $\lambda_{De}^{-1} > k_\perp >> \rho_i^{-1}$, and $k_\parallel \sim k_\perp \sqrt{m_e/m_i}$. The velocity-space scattering resulting from these fluctuations has been obtained by Baldwin-Callen,[11] and the form of their result when bounce-averaged is shown in Fig. 8. The basic scattering time scales as the electron drag time, t_{drag}, modified by the degree of wave amplification. The velocity dependence of the scattering is incorporated into the function $D(v_\perp)$, which has a maximum < O(1) in the positive slope of the ion distribution, is linear at small $v_\perp$, and decreases as $v_\perp^{-3}$ for large $v_\perp$. The number of wave-energy e-foldings A is conveniently expressed by a dimensionless quantity α{= max neg [yF(y)] in the notation of R-P}, which is a very sensitive function of the ion distribution, particularly at low energy where there exists the population inversion driving the mode. Electron temperature and the axial dependence of plasma parameters taken together reduce the values of

$$\left.\frac{\partial f}{\partial t}\right|_{B\text{-}C} \sim \frac{1}{v_\perp}\,\frac{\partial}{\partial v_\perp}\left(v_\perp D_{B\text{-}C}\,\frac{\partial f}{\partial v_\perp}\right)$$

$$D_{B\text{-}C} = \frac{\overline{v}^2}{t_{drag}}\;\frac{\hat{D}(v_\perp)}{\left(1+\omega_{pe}^2/\omega_{ce}^2\right)^2}\;e^A$$

$$A \equiv 2\int_{-L/2}^{L/2} ds\,\mathrm{Im}k_\parallel = \alpha\left(\frac{\omega_{pe}/\omega_{ce}}{\sqrt{1+\omega_{pe}^2/\omega_{ce}^2}}\;\frac{L}{\rho_i}\right)_{\text{midplane}}$$

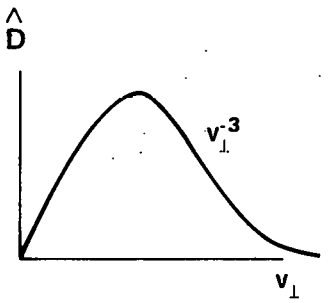

$$\alpha \gtrsim .08\;(R+1)^{-1/2}$$

$$\frac{L}{\rho_i} = \begin{cases} 125 \text{ in } 2\times \text{II} \\ 137 \text{ in MX} \end{cases}$$

Fig. 8. High-frequency convective loss-cone mode.

α from the R-P values by about 1/4, giving for collisional distribution $\alpha \approx 0.08(R + 1)^{-1/2}$, although this is increased for analytic models having an ambipolar cutoff. For scattering by these fluctuations not to exceed classical electron drag, A must be $\lesssim 5$, placing a limit on L/ρ_i of about $65(R + 1)^{1/2}$, where L is the total length, and ρ_i is the midplane Larmor radius in the actual magnetic field.

Just as for the diffusion in the quasilinear model of the drift-cone mode, the convective mode diffuses low-energy particles faster than high, as is shown by the velocity dependence of $D(v_\perp)$. Because of the sensitivity of α to the distribution and the uncertainty of relating diffusion in velocity space to particle lifetimes, it will be necessary to develop a velocity-space transport code, including axial dependence, to predict accurately the effects of this mode. A beginning in this direction has been made by Fader,[12] who added to LLL's HYBRID II (a two-dimensional Fokker-Planck code) a term similar to the scattering coefficient shown, without consideration of axial dependence. His results were surprising, showing a heating of ions and little loss of particles, and require reexamination.

The experimental evidence for this mode is limited; it is suspected of dominating the low-energy ("quiescent") runs in 2XII, but the mode identification was never complete. However, to the extent that the identification was valid, at $L/\rho_i = 125$ it conformed to the above-mentioned length limit and provides a basis for confidence in this scaling. As in 2XII, a concommitant of this scaling is the requirement that the local (β-enhanced) value of $\omega_{pe}^2/\omega_{ce}^2$ exceed unity, preferably by at least 3 or 4. Again, 2XII densities in this range decayed with $n\tau$ values close to the classical value for $T_i/T_e \approx 30$. Under stream-stabilized operation of 2XIIB, the mechanism of partially filling the loss cone, which is seen as stabilizing the drift-cone mode, also reduces the amplification of the

convective mode to the point that it would not be expected to dominate plasma loss. Under nonstabilized operation, of course, plasma loss is dominated by the ion-cyclotron noise.

At 50 keV and 12 kG central field, the proposed MX has an L/ρ_i value only 10% larger than that of 2XII, so with respect to this mode its behavior should be similar. Such experiments, which stabilize the drift-cone mode by increased plasma radius rather than by partial filling of the loss cone, permit investigation of the less-virulent convective mode. Present reactor designs exceed the estimated limit by a factor 3 for the large, 900-MW-output size and by 50% for the shorter 100-MW case. However, as has been emphasized above, the theory at this time is incomplete and is unable to assess all the ramifications of increased length, and the scaling of containment time with length has not been demonstrated experimentally.

Summary

The restrictions imposed by instabilities on mirror configurations can be summarized as follows:

- The mirror mode and the Alfvén ion-cyclotron mode provide a limit to the maximum beta attainable in a mirror configuration. Limitations on beta imposed by generating bad field curvature (ballooning interchange) have not been assessed. Such studies require high-beta, three-dimensional equilibria that are just beginning to be generated by our three-dimensional, guiding-center equilibrium codes.
- The minimum radius is determined from consideration of the DCLC mode. Confidence in our ability to parametrize the stability boundary for this mode is based on the ability of the quasilinear simulation to predict

the plasma evolution in 2XIIB. As yet, there is no experimental information as to how parameters change with increased radius. Such information will come from an MX experiment.

- Limits on the axial length are provided by the Rosenbluth-Post convective loss-cone mode and the negative-energy wave. Since the loss hole in velocity space was nearly filled in by the stabilizing stream or by the instability itself in the absence of the stream, and the experiment was dominated by ion-cyclotron noise, 2XIIB provided little information on the scaling of this mode. In the MX experiment, there is a lower required population of untrapped particles at marginal stability to DCLC, and the convective modes are expected to have a competitive influence on confinement.

Table 3 summarizes the present status of theory.

The present results indicate that with axial lengths projected for reactors, the maximum beta will be determined not by the mirror mode but rather by the Alfvén ion-cyclotron mode. However, as has also been pointed out, these results appear to be sensitive to the details of the distribution function, and qualitative predictions await calculations with realistic distributions.

The survey of the DCLC mode has shown that at moderately high beta, the minimum radius for stability is acceptable. One question that immediately arises is just how the boundary of the plasma (where beta is low and the radial scale length is short) can be stabilized. Suggestions put forth have been stream stabilization and gas or warm-plasma blankets; this is an area where further work is required.

The situation with regard to the convective loss-cone mode is in a partial state of flux in that rough scaling laws appear to be acceptable; however, as has been mentioned, answers are quite dependent upon details of

Table 3. Current theoretical estimate for reactor configuration.

Parameter	Controlling factor
$\beta = \frac{8\pi P_\perp}{Bv^2} \sim .7$	Mirror mode (Alfven ion cyclotron mode?)
$R_p/\rho_i \sim 40$	Drift cyclotron loss cone mode
$Lscale/\rho_i \sim 30$	Convective loss cone mode, negative energy mode(?)
$\frac{\omega_{pe}^2}{\omega_{ce}^2} \sim 3$	Convective loss cone mode
$E_i \sim 200$ keV	Reactor optimization
$E_e \sim .1\ E_i$	Ion-ion scattering

the distribution function, and these are presently under investigation. One result of this work not so dependent upon details of the distribution is the requirement that $(\omega_{pe}/\omega_{ce})^2$ exceed 3 or 4 to minimize scattering due to this mode. The negative-energy wave likewise requires further work. Results to date show that the flute-like mode leads to axial length comparable to the convective mode. Similar analysis on the higher axial mode remains to be done.

The final two entries in the table are a reminder of the energy range anticipated in a reactor. The last entry is a caution as to how important it is to avoid anomalous cooling on the electrons.

References

1. A. A. Galeev, in Third Conf. on Plasma Physics and Contr. Nucl. Fusion Res., Culham, England (IAEA, 1975), Vol. I, p. 341.
2. D. E. Baldwin, H. L. Berk, and L. D. Pearlstein, Turbulent Lifetimes in Mirror Machines, Lawrence Livermore Laboratory Rept. UCRL-77641 (1976).
3. W. C. Turner, W. F. Cummins, W. E. Nexsen, and E. J. Powers, Bull. Am. Phys. Soc. 20, 1232 (1975).
4. F. H. Coensgen, et al., Status of 2XIIB Plasma Confinement Experiments, Lawrence Livermore Laboratory Rept. UCID-17037 (1976).
5. R. C. Davidson and J. M. Ogden, Phys. Fluids 18, 1045 (1975).
6. For a list of references see J. G. Cordey and R. J. Hastie, Phys. Fluids 15, 2291 (1972).
7. H. L. Berk, et al., in Proc. Conf. on Plasma Physics and Controlled Nuclear Fusion (IAEA, 1969), Vol. II, p. 151.
8. D. E. Baldwin, et al., in Proc. Conf. on Plasma Physics and Contr. Fusion Research (IAEA, 1965), Vol. II, p. 151.

9. W. M. Tang, L. D. Pearlstein, and H. L. Berk, Phys. Fluids 15, 1153 (1972).

10. M. N. Rosenbluth and R. F. Post, Phys. Fluids 8, 547 (1965); R. F. Post and M. N. Rosenbluth, Phys. Fluids 9, 730 (1966).

11. D. E. Baldwin and J. D. Callen, Phys. Rev. Lett. 28, 1686 (1972).

12. W. J. Fader, Bull. Am. Phys. Soc. 20, 1249 (1975).

APPENDIX A. QUASILINEAR TRANSPORT MODEL FOR MIRROR MACHINES (H. L. Berk and J. J. Stewart)

In this Appendix, we describe the equations that govern the quasilinear transport model. In the first section, we describe the algebraic equations of the system, and in the second section we discuss the finite difference scheme for these equations.

Physical Equations

In mirror machines, the ion-velocity distribution is frequently sharply peaked perpendicular to the magnetic field. If one integrates over $v_\parallel$, one can then model the evolution of the distribution function $F(v_\perp^2,t)$, where $v_\perp$ is the perpendicular ion speed. Flute modes are only a function of $F(v_\perp^2,t)$, and a self-consistent quasilinear model can be constructed.

We use the following equation to describe the evolution of $F(v_\perp^2,t)$:

$$\frac{\partial F}{\partial t} = \frac{\partial}{\partial v_\perp^2} D(v_\perp^2) \frac{\partial F}{\partial v_\perp^2} + \nu_{DRAG} \frac{\partial}{\partial v_\perp^2} (v_\perp^2 F)$$

$$- \nu_{TRANSIT}(v_\perp^2)F + nS_{BEAM}(v_\perp^2) - F\int_0^\infty dv_\perp^2[1 - \alpha_{ION}(v_\perp^2)]S_{BEAM}(v_\perp^2)$$

$$+ S_{STRM}(v_\perp^2) - \nu_{CHX}(v_\perp^2)F + S_{CHX}(v_\perp^2)\int_0^\infty dv_\perp^2\, F(v_\perp^2)\nu_{CHX}(v_\perp^2) , \qquad (A1)$$

where the normalization is chosen so that $n/n_0 = 1/\bar{v}^2 \int_0^\infty dv_\perp^2\, F(v_\perp^2)$, n is the particle density, n_0 is a normalized density, and $\bar{v}$ is a normalized velocity. This equation is to be solved over a domain $0 < v_\perp^2 < v_{max}^2$ with the boundary conditions given by $\partial F(v_\perp^2 = 0)/\partial v_\perp^2 = F(v_\perp^2 = v_{max}^2) = 0$.

The first term on the right-hand side of Eq. (A1) is the quasilinear term, and $D(v_\perp^2)$ is the diffusion coefficient. This term will be discussed in detail below.

The second term is the electron drag with

$$\nu_{DRAG} = (8\pi^{1/2}\sqrt{2}/3)\, Z^2 n \ln \Lambda e^4 m^{1/2}/MT_e^{3/2},$$

where e is the electronic charge, m is the electron mass, M is the ion mass, Z the ion atomic number, and $\ln \Lambda$ is the Coulomb logarithm.

The third term, $\nu_{TRANSIT}(v_\perp^2)F$, is the loss term for particles in the loss cone. The loss region in a mirror is determined by the relation $v_\perp^2 < (v_\parallel^2 + q\Phi/M)$, where Φ is the ambipolar potential, $q = Z|e|$, and R is the mirror ratio. In this code, $v_\parallel^2$ can only be tracked in the mean, and we replace $v_\parallel^2$ with $2T_\parallel/M$. The untrapped particles can only remain in the mirror for a transit time, $\tau_{TRANSIT}$, which scales as $\tau_{TRANSIT} \sim L_p/[M/(T_\parallel + q\Phi)]^{1/2}$, where L_p is the axial scale length of the plasma. Hence, $\nu_{TRANSIT} = \alpha_T[(T_\parallel + q\Phi)/M]^{1/2}/L_p$, where α_T is a numerical constant that is typically taken as 0.5.

The next term, $nS_{BEAM}(v_\perp^2)$, is the beam input source and $S_{BEAM}(v_\perp^2) = I(v_\perp^2)(\sigma_{CHX} + \sigma_{ION})\ell/q$, where $\int dv_\perp^2\, I(v_\perp^2)$ is the neutral-beam current, σ_{CHX} the charge-exchange cross section, σ_{ION} the ionization cross section, and ℓ is the path length. For each beam particle input by charge exchange, a particle from the distribution is lost. This effect is represented by the term $-Fn_0 \int dv_\perp^2/\overline{v}^2\, [1 - \alpha_{ION}(v_\perp^2)]\, S_{BEAM}(v_\perp^2)$, where $\alpha_{ION} = \sigma_{ION}/(\sigma_{CHX} + \sigma_{ION})$.

A low-energy source $S_{ST}(v_\perp^2)$ is used to model the plasma stream that is injected axially into the plasma.

Particles may also be lost by charge exchange with the low-energy gas. We have treated the charge-exchange loss as if the low-energy gas can

penetrate the body of the plasma. This assumption is only marginally adequate in the 2XIIB experiment, but a more detailed model is too difficult to treat in this spatially zero-dimension code. We then take the loss of hot ions at a rate $\nu_{CHX}(v_\perp^2)$ and input cold ions with a source $S_{CHX}(v_\perp^2) \int dv_\perp^2 \, \nu_{CHX}(v_\perp^2)F$, such that $\int_0^\infty dv_\perp^2 \, S_{CHX}(v_\perp^2) = 1$.

In a mirror plasma, we expect the turbulence arising from the drift-cyclotron[A1,A2] mode to determine the quasilinear diffusion coefficient. The spectrum is characterized by $k_\parallel = 0$ and $k_\perp a_H \gtrsim 1$, where a_H is the mean ion Larmor radius, $k_\parallel$ the parallel wave number, and $k_\perp$ the perpendicular wave number. A difficulty in a straightforward application of quasilinear theory is that $k_\parallel = 0$ modes do not have any Landau damping in infinite-medium theory when magnetic field drifts are neglected. In order to avoid this problem, we introduce an ad hoc correlation frequency $\Delta\omega_k$. For two-dimensional turbulence, the quasilinear diffusion coefficient is then given by

$$D(v_\perp^2) = 4\pi \sum_{k,m} J_m^2\left(\frac{k_\perp v_\perp}{\omega_{ci}}\right) \left|\frac{q\phi_k}{M}\right|^2 \frac{m^2\omega_{ci}^2\Delta\omega_k}{[\omega(k) - m\omega_{ci}]^2 + \Delta\omega_k^2} , \qquad (A2)$$

where ϕ_k is the perturbed potential, ω_{ci} the ion-cyclotron frequency, and $\omega(k)$ the radian-oscillation frequency. If the noise is resonant near a cyclotron harmonic, then only one term in the sum on m in Eq. (A2) need be taken. If further we assume that the real part of the frequency is at the cyclotron frequency, the diffusion coefficient is then given by

$$D(v_\perp^2) = 4\pi \sum_k m^2 \frac{J_m^2\left(\frac{k_\perp v_\perp}{\omega_{ci}}\right)}{\Delta\omega_k} \left|\frac{q\phi_k}{M}\right|^2 \omega_{ci}^2 . \qquad (A3)$$

In this expression, the integer m is a function of k and is given by $m \doteq \omega(k)/\omega_{ci}$.

The correlation frequency consists of an intrinsic particle correlation rate (e.g., due to the transit rate of particles in an inhomogeneous magnetic field[A3] where $\Delta\omega_k \approx \omega_{ci} a_H (T_\perp/T_\parallel)^{1/2}/L$, where $L^{-1} = d \ln B/ds$, a_H the thermal Larmor radius, and $T_\perp$ and $T_\parallel$ the perpendicular and parallel ion temperatures), and a self-consistent turbulent correlation due to orbit diffusion. In the calculations to date, the correlation frequency is taken as an arbitrary constant. In future calculations, the correlation frequency will be taken as $\Delta\omega_k = k^2[D_0/\overline{v^2} + D(v_\perp^2)/v_\perp^2]$, where $D_0/\overline{v^2}$ is a constant. If $D_0 = 0$, $\Delta\omega_k$ is the correlation frequency due to spatial diffusion that has been used by Dupree. At low turbulent levels, $\Delta\omega_k$ is constant for a given k. We have chosen this form so that by using Eq. (A3) we may readily solve for $D(v_\perp^2)$. Substituting our assumed form for $\Delta\omega_k$ into Eq. (A3) yields

$$D(v_\perp^2) = -\frac{D_0 v_\perp^2}{2\overline{v^2}} + \left[\left(\frac{D_0 v_\perp^2}{2\overline{v^2}}\right)^2 + 4\pi v_\perp^2 \omega_{ci}^4 \sum_k \frac{m^2}{k^2} J_m \left|\frac{q\phi_k}{M}\right|^2\right]^{1/2}. \qquad (A4)$$

The amplitude $|\phi_k|^2$ is determined by the equation

$$\frac{\partial |\phi_k|^2}{\partial t} = 2\gamma(k)\ |\phi_k|^2 + \alpha(k)\ , \qquad (A5)$$

where $\gamma(k)$ is the growth rate, and $\alpha(k)$ is the intrinsic, low-level thermal fluctuation term. The growth rate is given by the expression

$$\frac{\gamma(k)}{\omega_{ci}} = \sigma_k \int_0^\infty dv_\perp^2\ \frac{\partial F}{\partial v_\perp^2}\ J_m^2\left(\frac{k_\perp v_\perp}{\omega_{ci}}\right)\ \frac{m^2 \omega_{ci}}{\Delta\omega_k}\ . \qquad (A6)$$

In the current investigation of this work, α_k and m were chosen arbitrarily because we wished to demonstrate that a typical self-consistent model would approach marginal stability. A more realistic form of $\omega(k)$ and $\gamma(k)$ for the drift-cone mode near marginal stability will be used for MX calculations.

The expressions for the rate of change of density and energy can be obtained by taking the appropriate moments of Eq. (A1). For the rate of density change we obtain

$$\frac{\partial n}{\partial t} = n_0 \int_0^{v_{max}^2} \frac{dv_\perp^2}{\bar{v}^2} \frac{\partial F(v_\perp^2)}{\partial t}$$

$$= \frac{n_0 D(v_{max}^2)}{\bar{v}^2} \frac{\partial F(v_{max}^2)}{\partial v_\perp^2} - n_0 \int_0^\infty \frac{dv_\perp^2}{\bar{v}^2} \nu_{TRANSIT}(v_\perp^2) F$$

$$+ n_0 \int_0^{v_{max}^2} \frac{dv_\perp^2}{\bar{v}^2} [\alpha_{ION}(v_\perp^2) S_{BEAM}(v_\perp^2) n + S_{STRM}(v_\perp^2)]. \qquad (A7)$$

The terms after the last equal sign in Eq. (A7) are, respectively: (1) the diffusive particle-loss term due to the absorbing high-energy boundary; (2) the transit-loss term of particles in the loss cone; (3) the particle input from the beam and stream. Note that there is no direct particle loss arising from electron drag or charge exchange. Normally, the diffusive loss term is a numerical loss term since an infinite energy domain cannot be treated analytically. However, in practice in a mirror machine there is a high-energy cutoff since the adiabatic invariant is no longer conserved at sufficiently high energy, and in some cases the high-energy boundary mocks up this effect.

Before we express the rate of change in kinetic energy,

$$\dot{TE} \equiv \frac{1}{2} M n_0 / \bar{v}^2 \int_0^{v_{max}^2} dv_\perp^2 v_\perp^2 \frac{\partial F}{\partial t},$$

we shall perform some algebraic manipulations with the diffusion term. When we construct TE from Eq. (A1), we obtain the following form from the diffusion term,

$$Q \equiv \frac{M}{2} n_0 \int_0^{v_{max}^2} \frac{dv_\perp^2}{\bar{v}^2} v_\perp^2 \frac{\partial}{\partial v_\perp^2} D(v_\perp^2) \frac{\partial F}{\partial v_\perp^2} .$$

If we integrate by parts, define $\omega_{pi0}^2 = 4\pi n_0 q^2/M$ and use Eqs. (A3), (A4), and (A6) Q can be written as

$$Q - \frac{n_0 M v_\perp^2}{2\bar{v}^2} D(v_\perp^2) \frac{\partial F}{\partial v_\perp^2} (v_\perp^2 = v_{max}^2)$$

$$= - \frac{M}{2\bar{v}^2} n_0 \int_0^{v_{max}^2} \frac{dv_\perp^2}{\bar{v}^2} D(v_\perp^2) \frac{\partial F}{\partial v_\perp^2}$$

$$= - \frac{2\pi q^2}{\bar{v}^2 M} n_0 \sum_k m^2 \int_0^{v_{max}^2} \frac{dv_\perp^2}{\bar{v}^2} \frac{J_m^2}{\Delta\omega_k} |\phi_k|^2 \omega_{ci}^2 \frac{\partial F}{\partial v_\perp^2}$$

$$= \frac{-\omega_{pi0}^2}{2\bar{v}^2} \sum_k \frac{\gamma_k}{\sigma_k} |\phi_k|^2 = \frac{-\omega_{pi0}^2}{4\bar{v}^2} \left(\sum_k \frac{1}{\sigma_k} \frac{\partial |\phi_k|^2}{\partial t} - \frac{\alpha k}{\sigma_k} \right). \qquad \text{(A8)}$$

We note that wave energy of the turbulence can be defined as

$$WE = \frac{\omega_{pi0}^2}{4\bar{v}^2} \sum_k \frac{1}{\sigma_k} \frac{\partial |\phi_k|^2}{\partial t} . \qquad \text{(A9)}$$

If we now construct $\dot{TE}$ from Eq. (A1) and use Eq. (A8), we obtain

$$\frac{\partial}{\partial t} (TE + WE) = \frac{\omega_{pi0}^2}{4\bar{v}^2} \sum_k \sigma_k \alpha_k$$

$$+ \frac{n_0 M v_\perp^2}{2\bar{v}^2} D(v_\perp^2) \frac{\partial F}{\partial v_\perp^2} (v_\perp^2 = v_{max}^2) - \nu_{DRAG} TE$$

$$- \dot{\overline{TE}}\Big|_{TRANSIT} + \dot{\overline{TE}}_{BEAM} - \dot{\overline{TE}}_{CHX} + \dot{\overline{TE}}_{STRM} , \qquad \text{(A10)}$$

where $\dot{\overline{TE}}_{TRANSIT}$ and $\dot{\overline{TE}}_{CHX}$ are the rate of energy lost by ions in the loss cone and from charge exchange with the low-energy neutral gas, while $\dot{\overline{TE}}_{BEAM}$

and $\dot{\overline{TE}}_{STRM}$ are the rate of energy input of the beam and stream, respectively. The precise forms of the $\dot{\overline{TE}}$ terms will be given below.

In Eq. (A10), the term $\omega_{pi0}^2/2\overline{v}^2 \sum_k \alpha_k/\sigma_k$ is the rate of work done on the plasma by the thermal fluctuations. Our theory is not refined enough to account for the fact that the work itself comes from plasma particles. However, this term can be made negligible by choosing α_k small enough.

The second term on the right-hand side of Eq. (A10) is the rate of energy lost by diffusion at the absorbing high-energy boundary.

The term $\nu_{DRAG}\overline{TE}$ is the energy lost to electrons through electron drag. The $\dot{\overline{TE}}$ terms are given by

$$\dot{\overline{TE}}_{TRANSIT} = \frac{n_0 M}{2} \int_0^{v_{max}^2} \frac{dv_\perp^2}{\overline{v}^2} v_\perp^2 \nu_{TRANSIT} F$$

$$\dot{\overline{TE}}_{BEAM} = \frac{n_0 M}{2} \int_0^{v_{max}^2} \frac{dv_\perp^2}{\overline{v}^2} v_\perp^2 S_b(v_\perp^2) n$$

$$- \frac{n_0 M}{2} \int_0^{v_{max}^2} \frac{dv_\perp^2}{\overline{v}^2} F v_\perp^2 \int_0^{v_{max}^2} \frac{dv_\perp^2}{\overline{v}^2} [1 - \alpha_{ION}(v_\perp^2) S_{BEAM}(v_\perp^2)]$$

$$\dot{\overline{TE}}_{CHX} = \frac{n_0 M}{2} \int_0^{v_{max}^2} \frac{dv_\perp^2}{\overline{v}^2} \nu_{CHX}(v_\perp^2) v_\perp^2 F$$

$$- \frac{n_0 M}{2} \int_0^{v_{max}^2} \frac{dv_\perp^2}{\overline{v}^2} v_\perp^2 S_{CHX}(v_\perp^2) \int_0^{v_{max}^2} \frac{dv_\perp^2}{\overline{v}^2} F(v_\perp^2) \nu_{CHX}(v_\perp^2)$$

$$\dot{\overline{TE}}_{STRM} = \frac{M n_0}{2} \int_0^{v_{max}^2} \frac{dv_\perp^2}{\overline{v}^2} v_\perp^2 S_{ST}(v_\perp^2) \ .$$

To complete our description, we need equations for the electron temperature and parallel ion temperature.

For the electron temperature, we use the equation that the rate of change of electron energy density is equal to the ion-to-electron power density transfer minus the power density lost out the mirror ends. The equation is expressed as

$$\frac{\partial}{\partial t}\left(\frac{3}{2} nT_e\right) = n\nu_{DRAG}T_i - \eta \frac{\partial n_L}{\partial t} T_e , \tag{A11}$$

where $\eta\ \partial n_L/\partial t\ T_e$ is the rate in which electron energy is lost out the ends of the mirror machine. Here, $\partial n_L/\partial t$ is the electron density loss rate, and ηT_e is the mean energy of a lost electron. Fokker-Planck calculations[A4] yield $\eta = 5$, while empirical 2X data suggest $\eta = 8$ is more realistic.

Note that from the quasineutrality condition, the rate in which electrons leave the mirror is equal to the rate in which the ions leave. Hence, from Eq. (A8),

$$\frac{\partial n_L}{\partial t} = n_0 \int_0^\infty \frac{dv_\perp}{\bar{v}^2} \nu_{TRANSIT}(v_\perp^2)F - n_0 D \frac{\left(v_{max}^2\right)}{\bar{v}^2} \frac{\partial F}{\partial v_\perp^2}(v_{max}^2). \tag{A12}$$

The ambipolar potential Φ is determined from a formula derived by Pastukhov,[A5] which is given by

$$\frac{dn_L}{dt} = \frac{2}{3}\left(\frac{M}{m}\right)\nu_{DRAG} \frac{RZ \exp\left(-\frac{q\Phi}{ZT_e}\right) T_e}{(2R + 1) \ln (4R + 2) q\Phi} . \tag{A13}$$

Typically, with stream, we find $q\Phi/T_e \approx 3$.

For the parallel ion temperature, we use a simple model which states that at finite beta, $\beta \equiv 8\pi nMv_\perp^2/B^2$, $T_\parallel$ needs to be greater than a minimum value $\alpha\beta T_\perp$. In this investigation, we use $T_\parallel = \alpha\beta T_\perp$, with α chosen arbitrarily. For a more realistic treatment of $T_\parallel$ to both the mirror condition and ion-ion collisions, a two-dimensional velocity phase space is needed. Such a calculation is currently being developed by Rognlien.

Finite-Difference Scheme

Equation (A1) is solved by numerical-difference equations. The grid is taken with an arbitrary spacing such that we have a list of points $0 \leq j \leq J + 1$ and

$$x_{j+1} = x_j + \Delta x_j + \Delta x_{j+1} , \tag{A14}$$

where $x_j = v_\perp^2/\bar{v}^2$, and Δx_j is a predetermined interval with the constraints that $\Delta x_0 = \Delta x_1$, $\Delta x_J = \Delta x_{J+1}$, $x_0 = -\Delta x_0$, and $v_{max}^2 = \bar{v}^2(x_J + \Delta x_J)$. The boundary conditions for $F_j \equiv F(v_\perp^2)$ are chosen such that $F_0 = F_1$ and $F_J = -F_{J+1}$. In finite difference form, our normalization condition is

$$\int_0^{v_{max}^2} \frac{dv_\perp^2}{\bar{v}^2} F(v_\perp^2) \equiv \sum_{j=1}^{J} \delta_j F_j = n/n_0 , \tag{A15}$$

where $\delta_j = (\Delta x_{j-1} + 2\Delta x_j + \Delta x_{j+1})/2$, and n_0 is taken as the initial plasma density. Equation (A15) can be derived from the trapezoidal rule. The end effects of the trapezoidal rule are simplified in Eq. (A15) due to our boundary conditions. The first moment of F, which is needed to construct the kinetic energy, is expressed as

$$n_0 \int_0^{v_{max}^2} dv_\perp^2 \frac{v_\perp^2}{\bar{v}^4} F(v_\perp^2) \equiv n_0 \sum_{j=1}^{J} \delta_j x_j F_j \equiv n\bar{x} . \tag{A16}$$

The differential terms in Eq. (A1) are represented as follows:

$$\text{(Term 1)} \qquad \frac{\partial F}{\partial t} \equiv \frac{1}{\Delta t}\left(F_j^n - F_j^0\right) , \tag{A17}$$

where $F_j^n = F(x_j\bar{v}^2, t + \Delta t)$, $F_j^0 = (x_j\bar{v}^2, t)$. This representation is second-order accurate in Δt.

(Term 2) $$\frac{\partial}{\partial v_\perp^2} D(v_\perp^2) \frac{\partial}{\partial v_\perp^2} F \equiv$$

$$\frac{1}{\bar{v}^4} \delta_j \left[\frac{D_{j+1} (\bar{F}_{j+1} - \bar{F}_j)}{\Delta x_j + \Delta x_{j+1}} - \frac{D_j (\bar{F}_j - \bar{F}_{j-1})}{\Delta x_j + \Delta x_{j-1}} \right] , \tag{A18}$$

where $\bar{F}_j = (F_j^n + F_j^0)/2$. For D_j, we use the expression given by Eq. (A3) with $v_\perp^2 = \bar{v}^2(x_j + \Delta x_j)$. Equation (A18) is accurate to second order in time and second order in velocity space if the grid is uniform on first order in velocity space for a nonuniform grid.

In the code, we do not use Bessel functions because it is time consuming to generate or space consuming to store. Further, physically the oscillations of the Bessel function can be expected to be smoothed over by the spatial variations of the system. Hence, we use a form that reproduces the form of the square of the Bessel function for small argument and the average of the square of the Bessel function for large argument. In particular, we choose the form

$$\tilde{J}_n^2(y) = F_n(y)\, H(y)/[F_n(y) + H(y)] , \tag{A19}$$

where $F_n(y) = [(y/2)^n/n!]^2$ and $H(y) = (\pi y)^{-1}$.

The expression,

$$\psi_k = \left| \frac{q\phi_k}{M\bar{v}^2} \right|^2 ,$$

needed in D_j, is evaluated at $t + \Delta t/2$. The finite difference form we use for the time evolution of ψ, given by Eq. (A5), is

$$\psi_k \left(t + \frac{\Delta t}{2}\right) - \psi_k \left(t - \frac{\Delta t}{2}\right) = \gamma(k,t) \left[\psi_k \left(t + \frac{\Delta t}{2}\right) + \psi_k \left(t - \frac{\Delta t}{2}\right) \right] + \tilde{\alpha}_k \Delta t , \tag{A20}$$

where $\tilde{\alpha}_k = q^2 \alpha_k / (M\bar{v}^2)^2$. The finite difference form of $\gamma(k,t)$ is given by

$$\frac{\gamma(k,t)}{\omega_{ci}} = m^2\sigma_k\omega_{ci}\left\{\sum_{j=1}^{J-1}\frac{(F_{j+1}-F_j)\,\tilde{J}_m^2\left[\frac{k\bar{v}}{\omega_{ci}}(x_{j+1}+x_j)^{1/2}\right]}{\Delta\omega_k}\right.$$

$$\left. + \frac{F_J\tilde{J}_m^2}{\Delta\omega_k}\left(\frac{kv_{max}}{\omega_{ci}}\right)\right\} . \qquad (A21)$$

The conservation laws of the zeroth and first moments of the diffusion term given by Eq. (A18) can now be considered. We have that the change of n/n_0 due to the diffusion term is

$$\frac{n^n}{n_0} - \frac{n^0}{n_0} = \frac{\Delta t}{v^4}\sum_{j=1}^{J}\left[\frac{D_{j+1}(\bar{F}_{j+1}-\bar{F}_j)}{(\Delta x_j+\Delta x_{j+1})} - \frac{D_j(\bar{F}_j-\bar{F}_{j-1})}{(\Delta x_j+\Delta x_{j-1})}\right] = -\frac{\Delta t}{v^4}\,\frac{D_{J+1}\bar{F}_J}{\Delta x_J} . \qquad (A22)$$

In obtaining the result in Eq. (A22), we have used $F_1 = F_0$ and $F_J = -F_{J+1}$ and $\Delta x_J = \Delta x_{J+1}$. Observe that our finite difference scheme for the diffusion conserves particles except for the leakage at the edge of the grid.

For the change in $n\bar{x}$ due to diffusion, we have

$$\left(\frac{n\bar{x}}{n_0}\right)^n - \left(\frac{n\bar{x}}{n_0}\right)^0 = \frac{\Delta t}{v^4}\left[\sum_{j=1}^{J}\frac{x_jD_{j+1}(\bar{F}_{j+1}-\bar{F}_j)}{\Delta x_j+\Delta x_{j+1}} - \frac{x_jD_j(\bar{F}_j-\bar{F}_{j-1})}{\Delta x_j+\Delta x_{j-1}}\right]$$

$$= -\frac{\Delta t}{v^4}\sum_{j=1}^{J-1}D_{j+1}(\bar{F}_{j+1}-\bar{F}_j) + \frac{\Delta t}{v^4}D_{J+1}\frac{x_J\bar{F}_J}{\Delta x_J}$$

$$= -4\pi\Delta t\omega_{ci}^2\sum_k m^2\psi\left(t+\frac{\Delta t}{2}\right)\left[\sum_{j=1}^{J-1}\frac{\tilde{J}_m^2(\bar{F}_{j+1}-\bar{F}_j)}{\Delta\omega_k} + \frac{J_m^2\left(\frac{kv_m^2}{\omega_{ci}}\right)\bar{F}_J}{\Delta\omega_k}\right]$$

$$- \frac{\Delta t}{v^4}(x_J+\Delta x_J)D_{J+1}\,\bar{F}_J/\Delta x_J$$

$$= -2\pi\sum_k\frac{\Delta t\psi_k\left(t+\frac{\Delta t}{2}\right)}{\sigma_k}[\gamma_k(t+\Delta t)+\gamma_k(t)]$$

$$- \frac{\Delta t}{v^4}(x_J+\Delta x_J)D_{J+1}\,\bar{F}_J/\Delta x_J . \qquad (A23)$$

Using Eq. (A23), we find that the change in kinetic and wave energy in the finite-difference scheme due to diffusion is

$$\mathrm{TE}(t + \Delta t) + \mathrm{WE}\left(t + \frac{\Delta t}{2}\right) - \mathrm{TE}(0) - \mathrm{WE}\left(\frac{-\Delta t}{2}\right)$$

$$= -n_0 \sum_{\Delta t} \left(\frac{M v_{max}^2}{2} D_{J+1} \frac{\overline{F}_J}{\Delta x_j} - \tilde{\alpha}_k \sigma_k \frac{M\overline{v}^2}{2} \right)$$

$$-\Delta t \sum_k \gamma_k(t + \Delta t)\, \mathrm{WE}_k\left(t + \frac{\Delta t}{2}\right) - \Delta t \sum_k \gamma_k(0)\, \mathrm{WE}(0), \qquad \text{(A24)}$$

where $\sum_k \mathrm{WE}_k = \mathrm{WE}$. This equation states that the loss of total energy is due to kinetic energy flowing out the end of the grid plus the work done by the fluctuations to initiate the wave energy. In addition, there is a small phase term that corrects itself with each time step.

For the drag, we use the following difference scheme:

$$\text{(Term 3)} \qquad \nu_{DRAG} \frac{\partial}{\partial v_\perp^2} (v_\perp^2 F)$$

$$= \frac{\nu_{DRAG}}{4\delta_j} [(x_j + x_{j+1})(\overline{F}_{j+1} + \overline{F}_j)(1 - \delta_{j,J})$$

$$- (x_j + x_{j-1})(\overline{F}_j + \overline{F}_{j-1})], \qquad \text{(A25)}$$

where $\delta_{j,J}$ is the Kroneker-delta. This expression is second-order accurate in Δt and second-order accurate in Δx if Δx is uniform or first order in Δx if Δx is nonuniform.

It readily follows that the zeroth moment of Eq. (A25) is exactly zero (note that $x_0 + x_1 = 0$). For the change in the first moment due to the drag, we have

$$\left(\frac{n\bar{x}}{n_0}\right)^n - \left(\frac{n\bar{x}}{n_0}\right)^0$$

$$= \frac{\nu_{DRAG}\Delta t}{4} \sum_{j=1}^{J-1} x_j(x_j + x_{J+1})(\bar{F}_{j+1} + \bar{F}_j) - x_j(x_j + x_{j-1})(\bar{F}_j + \bar{F}_{j-1})$$

$$= -\frac{\nu_{DRAG}\Delta t}{4} \sum_{j=1}^{J-1} (\Delta x_j + \Delta x_{j+1})(x_j + x_{j+1})(\bar{F}_{j+1} + \bar{F}_j) \qquad \text{(A26)}$$

Equation (A26) is the finite-difference form of the statement that the decrease of the kinetic energy due to drag is the energy absorbed by electrons. Note that the right-hand side of Eq. (A26) is not exactly proportional to $n\bar{x}$ but differs from $n\bar{x}$ to order $(\Delta x)^2$ for a uniform grid or to order Δx for a nonuniform grid.

To represent the transit loss term and stream term, we use the form

$$\text{(Term 4)} \quad S_{STRM}(\bar{v}^2 x_j) - \nu_{TRANSIT}(\bar{v}^2 x_j)F(v^2) \equiv S_{STRMj} - \nu_{TRANSIT}(j)\bar{F}_j. \qquad \text{(A27)}$$

This form is accurate to second order in Δt and Δx. The change in the zeroth and first moments due to this term are

$$\frac{n^n}{n_0} - \frac{n^0}{n_0} = -\Delta t \sum_j \delta_j[\nu_{TRANSIT}(j)\,\bar{F}_j - S_{STRMj}]$$

$$\frac{(nx)^n}{n_0} - \frac{(n\bar{x})^0}{n_0} = -\Delta t \sum_j \delta_j x_j[\nu_{TRANSIT}(j)\,\bar{F}_j - S_{STRMj}]. \qquad \text{(A28)}$$

(Term 5) We cannot readily maintain second-order time accuracy in the beam source since it is proportional to the density. If we attempted a central time difference scheme on the density, we would need to solve implicitly a full $J \times J$ matrix. To avoid this complication, we use the previous density in our source. In order to conserve particles, we also introduce this time lag into the charge-exchange loss. Thus, we use the following finite difference representation:

$$S_{BEAM}(\bar{v}^2 x_j)n - \int_0^{v^2_{max}} dv_\perp^2 \, [1 - \alpha_{ION}(\bar{v}^2 x_j)] \, S_{BEAM}(v_\perp^2)F$$

$$\equiv S_{BEAMj} - \sum_{j=1}^{J} \delta_j (1 - \alpha_{IONj}) \, S_{BEAMj} \, . \tag{A29}$$

The changes in the zeroth and first moments due to these terms are

$$\begin{aligned} \frac{n^n}{n_0} - \frac{n^0}{n_0} &= \Delta t \sum_j \delta_j \alpha_j F_j^0 \, S_{BEAMj} \\ \frac{(n\bar{x})^n}{n_0} - \frac{(n\bar{x})^0}{n_0} &= \Delta t n^0 \sum_{j=1}^{J} \delta_j x_j \, S_{BEAMj} \\ &\quad - \Delta t \sum_{i=1}^{J} \delta_i x_i F_i \sum_{j=1}^{J} \delta_j (1 - \alpha_i) S_{bj} \, . \end{aligned} \tag{A30}$$

(Term 6) Similarly, the charge exchange with background neutral gas is offset in time to avoid inverting a large matrix. The charge-exchange term is represented by

$$-\nu_{CHX}(\bar{v}^2 x_j) \, F(\bar{v}^2 x_j) + S_{CHX}(\bar{v}^2 x_j) \int_0^{v^2_{max}} dv_\perp'^2 \, F(v_\perp'^2) \, \nu_{CHX}(v_\perp'^2)$$

$$= -\nu_{CHXj} F_j^0 + S_{CHXj} \sum_{j=1}^{J} \delta_j F_j \, \nu_{CHXj} \, , \tag{A31}$$

where $\sum_{j=1}^{J} S_{CHXj} \delta_j = 1$. Equation (A31) conserves n while the change it induces in $n\bar{x}/n_0$ is given by

$$\begin{aligned} \left(\frac{n\bar{x}}{n_0}\right)^n - \left(\frac{n\bar{x}}{n_0}\right)^0 &= - \sum_{j=1}^{J} \delta_j x_j \, \nu_{CHXj} F_j^0 \\ &\quad + \sum_{i=1}^{J} \delta_i x_i S_{CHXi} \sum_{j=1}^{J} \delta_j F_j \nu_{CHXj} \, . \end{aligned} \tag{A32}$$

The finite-difference equation we have generated produces an implicit tridiagonal matrix for the unknown F_j^n for $0 < j < J$ with the boundary condition $F_0^n = F_1^n$ and $F_J^n = -F_{J+1}^n$. This equation is solved by a standard tridiagonal Gaussian reduction technique.

For the change in the electron temperature, we integrate Eq. (A1) over a time interval Δt. This yields

$$\frac{3}{2}(nT_e)^n - \frac{3}{2}(nT_i)^0 = \int_t^{t+\Delta t} n\nu_{DRAG}T_i - \frac{\eta\Delta n_L[(nT_e)^n + (nT_e)^0]}{(n^n + n^0)} . \quad (A33)$$

The term $\int_t^{t+\Delta t} n\nu_{DRAG}T_i$ is the energy transferred from ions to electrons and it is given by the last term of Eq. (A26) multiplied by $M\bar{v}^2/2$. The second term on the right-hand side of Eq. (A33) is the electron energy lost axially and Δn_L is given by [see Eqs. (A22) and (A28)]

$$\Delta n_L = n_0\Delta t \sum_j \delta_j \nu_{TRANSIT}(j)\bar{F}_j + \frac{\Delta t}{\bar{v}^4}\frac{D_{J+1}\bar{F}_J}{\Delta x_J} . \quad (A34)$$

Finally, the ambipolar potential which is governed by Eq. (A13), is determined by a Newton-Rhapson iteration procedure after $\partial n_L/\partial t$ is replaced with $\Delta n_L/\Delta t$ [see Eq. (A34)].

References

A1. R. F. Post and M. N. Rosenbluth, Phys. Fluids 9, 730 (1966).

A2. D. E. Baldwin, H. L. Berk, and L. D. Pearlstein, Turbulent Lifetimes in Mirror Machines, Lawrence Livermore Laboratory Rept. UCRL-77641 (1976).

A3. D. E. Baldwin, C. O. Beasley, H. L. Berk, W. M. Farr, R. C. Harding, J. E. McCune, L. D. Pearlstein, and A. Sen, in Proc. 4th Int. Conf. on Plasma Physics and Contr. Nucl. Fus. Res., Madison, WI (IAEA, 1971), Vol. II, p. 735.

A4. A. H. Futch, Jr., J. P. Holdren, J. Killeen, and A. A. Mirin, Plasma Phys. 14, 211 (1972).

A5. V. P. Pastukhov, Nucl. Fusion 14, 3 (1974).

APPENDIX B. SELF-CONSISTENT TURBULENT DIFFUSION IN THE TWO-DIMENSIONAL HYBRID II CODE (T. D. Rognlien and T. A. Cutler)

Introduction

The HYBRID II Fokker-Planck code has been modified to include the effect of turbulent diffusion as caused by electrostatic oscillations. The model used is that developed by Berk and Stewart for their one-dimensional Fokker-Planck code. In this quasilinear model, the oscillations grow due to the loss-cone nature of the distribution function, and those oscillations in turn drive the distribution function to marginal stability through turbulent diffusion. The calculation is self-consistent in the sense that energy is conserved between the waves and the particles. The model gives a growth rate that is a reasonable approximation to that for the drift loss-cone instability. Below, we give a brief description of the form that the diffusion operator and the growth rate take in spherical velocity coordinates as used by HYBRID II and discuss the new effects that this two-dimensional code can model.

Diffusion Operator and Growth Rate in Spherical Coordinates

A general velocity diffusion term, $\underset{\approx}{D}$, enters the Fokker-Planck equation in the following way:

$$\frac{\partial f}{\partial t} = \nabla_v \cdot \underset{\approx}{D} \cdot \nabla_v f + \text{classical collision terms.} \tag{B1}$$

For electrostatic waves propagating perpendicular to the magnetic field, one has

$$\underset{\approx}{D} = D_{\perp} \hat{i}_{\perp} \hat{i}_{\perp} , \tag{B2}$$

where $D_\perp$ is given by*

$$D_\perp(v_\perp) = \frac{\pi q^2}{m_i^2 v_\perp^2} \, n^2 \omega_{ci}^2 \, \frac{d^2 k_\perp}{(2\pi)^2} \, |\phi_{k_\perp}|^2 \, J_n^2 \, \frac{k_\perp \omega_\perp}{\omega_{ci}} \, \frac{\Delta\omega_k}{(\omega_k - n\omega_{ci})^2 + \Delta\omega_k^2} \, . \qquad \text{(B3)}$$

Here, $\Delta\omega_k$ is the correlation frequency. By using Eq. (B2), one finds the diffusion term of the Fokker-Planck equation in spherical coordinates to be

$$\nabla_v \cdot \underset{\approx}{D} \cdot \nabla_v f = \frac{1}{v^2} \frac{\partial}{\partial v} D_\perp (v \sin\theta) \left(v^2 \sin^2\theta \frac{\partial f}{\partial v} + v \sin\theta \cos\theta \frac{\partial f}{\partial \theta} \right)$$

$$+ \frac{1}{v^2 \sin\theta} \frac{\partial}{\partial \theta} D_\perp (v \sin\theta) \left(v \sin^2\theta \cos\theta \frac{\partial f}{\partial v} + \sin\theta \cos^2\theta \frac{\partial f}{\partial \theta} \right) \, . \qquad \text{(B4)}$$

These terms have now been added to the existing HYBRID II code.

The growth rate is found by multiplying Eq. (B4) by $\frac{1}{2} m_i v_\perp^2$ and then integrating over velocity space. This energy integral is then proportional to the growth rate, γ, since the rate of energy change for the waves is 2γ times the wave energy. This insures that energy is conserved between the waves and the particles. The constant of proportionality can be obtained from a more detailed analysis of the linear dispersion relation. However, energy is conserved independent of the value of this constant, and only the time scale of the wave growth is affected by it. After integrating by parts, we find the growth rate in spherical coordinates

$$\gamma_{k_\perp} = K \left[\int_0^{\frac{\pi}{2}} \int_0^\infty \sum_n \frac{n^2 J_n^2 \left(\frac{k_\perp v_\perp}{\omega_{ci}} \right)}{v_\perp^2} \, \frac{\Delta\omega_k}{(\omega_k - n\omega_{ci})^2 + \Delta\omega_k^2} \right.$$

$$\left. \cdot \, v^2 \sin^2\theta \left(v \sin\theta \frac{\partial f}{\partial v} + \cos\theta \frac{\partial f}{\partial \theta} \right) \right] dv d\theta \, , \qquad \text{(B5)}$$

where K is a constant. The wave amplitudes are then allowed to grow at this rate; i.e.

---

*R. C. Davidson, Methods in Nonlinear Plasma Theory (Academic Press, NY, 1972), p. 166.

$$\frac{d}{dt} |\tilde{\phi}_k|^2 = 2\gamma_k |\tilde{\phi}_k|^2 + \text{FLUC}, \tag{B6}$$

where FLUC is a small, constant, background-noise level.

The code is thus to be run in the same way as the one-dimensional code: several waves at different $k_\perp$'s are chosen and assumed to have a frequency very near one of the cyclotron harmonics so that only one term in the sum over n is used for each wave [see Eqs. (B3) and (B5)]. It should also be mentioned that as in the one-dimensional code, we have the capability of using any mixture of the exact Bessel function and the envelope of the Bessel function.

New Effects to be Studied with the Two-Dimensional Code

Pitch-Angle Scattering

The major effect to be studied with the two-dimensional code is that of pitch-angle scattering. This effect could be significant near the loss-cone boundary since the particles there have lower velocities and pitch-angle scatter somewhat more effectively. Also, particles that cross the loss-cone boundary with significant parallel velocity are more energetic and thus represent more of an energy loss than a particle loss. The code has an end-loss diagnostic that gives the energy spectrum of these particles leaving the system.

Separate Calculation of Stream and Plasma Distribution Functions

The HYBRID II code has the option of using multispecies. Thus, the stream could be considered one species and the target plus beams as the second species. This would help answer the question of whether or not the stream is actually trapped by rf or simply flows through the system.

Non-Maxwellian Electrons

The code also has the option of "Fokker-Plancking" the electrons. We have some preliminary results indicating that the electrons are non-Maxwellian, which affects the drag on ions. It is not clear how large this effect is, however.

Off-Angle, Neutral-Beam Injection

Since off-angle, neutral-beam injection may be favorable from a β-limit point of view, the two-dimensional code offers the ability to determine the effect of such injection on the stability of the plasma and the associated loss rates.

APPENDIX C. WARM-PLASMA STABILIZATION OF DRIFT-CONE MODE AT FINITE BETA* (H. L. Berk and M. J. Gerver†)

Mirror plasmas are susceptible to the drift cyclotron loss mode[C1] if the radial scale length is sufficiently short. Post[C2] has estimated the amount of warm plasma that is necessary to stabilize this mode in the low beta limit. Tang et al.[C3] show that at finite beta there is appreciable stabilizing tendency, although appreciable scale lengths are still needed for stability. In this note, we calculate the fraction of warm plasma $\Delta \equiv n_w/n_H$ that is necessary to stabilize the drift cone mode at finite beta. Here H refers to the confined "hot" plasma and w to unconfined "warm" plasma.

For the distribution function we choose the form

$$F(v_\perp) = \left(v_H^2 - v_h^2\right)^{-1} \left[\exp\left(-\frac{v_\perp^2}{v_H^2}\right) - \exp\left(-\frac{v_\perp^2}{v_h^2}\right)\right] + \frac{\Delta}{v_w^2} \exp\left(-v^2/v_w^2\right). \tag{C1}$$

We see that the loss cone nature of the distribution is simulated by a "hole" velocity v_h. Physically, this hole velocity can be interpreted as $1/2\ M_i\ v_h^2 \simeq q\Phi + \alpha T_\parallel$, where q is the electronic charge, Φ the ambipolar potential, $T_\parallel$ the parallel temperature, and α a constant of order unity.

The dispersion relation for a $k_\parallel = 0$ mode and finite beta in the limit $\frac{\omega\omega_{ci}}{k_\perp v_i^2} < 1$, can be written as

---

*Originally published as Lawrence Livermore Laboratory Rept. UCRL-77711 dated January 13, 1976.

†Electronics Research Laboratory, University of California, Berkeley, California 94720.

$$
\begin{aligned}
&(1+\Delta)\left[-\frac{\varepsilon}{\xi}(1+\beta/2)+\beta+\left(\frac{m}{M}+\frac{\omega_{ci}^2}{\omega_{pi}^2}\right)k_\perp^2 a_H^2\right] \\
&+2\left[\xi Z_R(\xi)\left(1-\frac{\omega_H^*}{\omega}\right)-2\xi\frac{v_H}{v_h}Z_R\left(\xi\frac{v_H}{v_h}\right)\left(1-\frac{\omega_h^*}{\omega}\right)\right]\left(\frac{v_H^2}{v_H^2-v_h^2}\right) \\
&+2\Delta\frac{v_H^2}{v_w^2}\left[Z_R\left(\xi\frac{v_H}{v_w}\right)\left(1-\frac{\omega_w^*}{\omega}\right)\xi\frac{v_H}{v_w}+1\right] \qquad \text{(C2)} \\
&+2\pi^{1/2}\cot\left(\frac{\pi\omega}{\omega_{ci}}\right)\xi\left\{\frac{v_H^3}{(v_H^2-v_h^2)}\left[\frac{\exp}{v_h}\left(-\xi^2\frac{v_H^2}{v_h^2}\right)\left(1-\frac{\omega_h^*}{\omega}\right)\right.\right. \\
&\left.\left.-\left(1-\frac{\omega_H^*}{\omega}\right)\frac{1}{v_H}\exp(-\xi^2)\right]-\Delta\frac{v_H^3}{v_w^3}\left(1-\frac{\omega_w^*}{\omega}\right)\exp\left(-\xi^2\frac{v_H^2}{v_w^2}\right)\right\}=0,
\end{aligned}
$$

where $\xi=\frac{\omega}{k_\perp v_H}$, $a_H=v_H/\omega_{ci}$, $\varepsilon=\frac{a_H}{R_p}$, R_p is the radial scale length, $\beta=\frac{\omega_{pi}^2 v_H^2}{\omega_{ci}^2 c^2}$, $Z_R(y)=\frac{1}{\pi^{1/2}}P\int\frac{dx\,\exp(-x^2)}{(x-y)}$, and $\omega_j^*=\frac{k_\perp v_j^2}{2\omega_{ci}R_p}$.

Frequently one may replace $\cot\left(\frac{\pi\omega}{\omega_{ci}}\right)$ with -i. This replacement is justified when $\mathrm{Im}\,\omega > \omega_{ci}$[C1] or when the magnetic field drift, v_D, is taken into account and $k_\perp v_D > \omega_{ci}$.[C4] This last inequality is usually realized so that in Eq.(C2) we shall henceforth use -i rather than $\cot(\pi/\omega_{ci})$. In this case, the dispersion relation is identical with the straight-line orbit approximation.

Other subsidary approximations that are convenient in our analytic analysis are $\Delta \ll 1$, $\frac{v_h}{v_H}\ll 1$, $\xi\frac{v_H}{v_h}\ll 1$, and $\frac{\omega_H^*}{\omega}\ll 1$. We also redefine ε to include the factor $1+\beta/2$ (then ω_H^* would be $k_\perp v_H^2/[\omega_{ci}R_p(2+\beta)]$). Then Eq.(C2) becomes

$$
-\frac{\varepsilon}{\xi}+\beta+\left(\frac{m}{M}+\frac{\omega_{ci}^2}{\omega_{pi}^2}\right)(k_\perp a_H)^2-\Delta\frac{v_H^2}{v_w^2}Z_R'\left(\xi\frac{v_H}{v_w}\right)
$$

$$- i \frac{v_H}{v_h} \pi^{1/2} \xi \left[1 - \Delta \frac{v_h v_H^2}{v_w^3} \exp \left(- \xi^2 \frac{v_H^2}{v_w^2} \right) \right] = 0 . \qquad \text{(C3)}$$

At moderately high β, $\beta > \beta_c \equiv \left(\frac{v_H}{v_h}\right)^{2/3} \left(\frac{m}{M} + \frac{\omega_{ci}^2}{\omega_{pi}^2}\right)^{1/3}$, and $\eta = 0$, this dispersion relation has been analyzed by Tang et al.[C3] The stability condition is found to be $\varepsilon \leq 2\beta^{1/2} \left[\frac{\omega_{ci}^2}{\omega_{pi}^2} + \frac{m}{M} \right]^{1/2} \equiv \varepsilon_{cr}$.

For $\varepsilon > \varepsilon_{cr}$, the drift cone mode is unstable, and we need warm plasma to stabilize this mode. The marginal condition is obtained by equating the real and imaginary parts. We obtain

$$1 = \Delta \frac{v_h v_H^2}{v_w^3} \exp \left(- \xi^2 v_H^2 / v_w^2 \right) \qquad \text{(C4)}$$

$$\Delta \frac{v_H^2}{v_w^2} Z_R' \left(\xi \frac{v_H}{v_w} \right) = \frac{-\varepsilon}{\xi} + \beta + \left(\frac{m}{M} + \frac{\omega_{ci}^2}{\omega_{pi}^2} \right) k_\perp^2 a_H^2 . \qquad \text{(C5)}$$

For long wavelengths and $\varepsilon >> \varepsilon_{cr}$, the last term in Eq. (C5) may be neglected. (We consider shorter wavelengths later.) For sufficiently small β, we may also neglect the β term. We then eliminate v_w and find

$$\Delta = \left(\frac{v_h}{v_H} \right)^{1/2} \varepsilon^{3/2} \left[\frac{\exp(-y^{2/3})}{-y Z_R'(y)} \right]^{3/2} ,$$

where $y = \xi \frac{v_H}{v_w}$. The minimum Δ occurs for $y \doteq 0.5$ and $\Delta_{min} = 2\varepsilon^{3/2} (v_h/v_H)^{1/2}$.

One can infer from our marginal stability condition that $\xi \frac{v_H}{v_h} \sim \left(\varepsilon \frac{v_H}{v_h} \right)^{1/2}$, and hence we require $\varepsilon > v_h/v_H$ to justify Eq. (C3). We shall discuss below

the case when this inequality is violated.

As β is increased, it becomes competitive in Eq. (C6) when $\beta \sim \left(\frac{v_H}{v_h}\,\varepsilon\right)^{1/2} \equiv \beta_1$. For $\beta > \beta_1$, the first two terms on the right-hand side of Eq. (C6) are dominant, so that we have $\beta = \varepsilon/\xi$ or $v_w = v_H\varepsilon/y\beta$. Eliminating v_w from Eq. (C4) yields

$$\Delta = v_H\varepsilon^3 / \left[y^3 \exp(-y^2)\, v_h\, \beta^3 \right] \quad \text{and} \quad \Delta_{min} = 2.4\, v_H\varepsilon^3/v_h\, \beta^3 \quad \text{for } y = (3/2)^{1/2}.$$

In the case $\varepsilon \gtrsim v_h/v_H$, so that the phase velocity of the unstable wave is comparable to v_h, it is necessary to fill in the entire loss cone with warm plasma. Simultaneously, ω_H^* becomes comparable with ω so that the ion density gradient becomes a drive for the instability as well. In this regime, the minimum density of warm plasma necessary for stabilization is found numerically from Eq. (C2). The results are shown in Fig. C-1 and very roughly the fraction of warm plasma needed is $\Delta = \left(v_h/v_H\right)^2$.

To compute the curves in Fig. C-1 in the region $\varepsilon \sim \varepsilon_{cr}$, we have chosen $\omega = \omega_{ci}$. When the last term in Eq. (C5) may be neglected, the marginal stability curves depend only on $\xi = \omega/k_\perp v_H$, and hence ω can be chosen arbitrarily. When $\varepsilon \sim \varepsilon_{cr}$, the choice $\omega = \omega_{ci}$ reproduces Tang's result quite closely.

In summary, in this analysis we have considered three regimes of instability. For regime (1), $2\left(\frac{m}{M}\,\beta\right)^{1/2} \lesssim \varepsilon \lesssim \beta^2\, v_h/v_H$, stability is achieved for

$$\Delta \geq 2.4 \left(\frac{v_H}{v_h}\right)\frac{\varepsilon^3}{\beta^3} \quad . \tag{C6}$$

For regime (2), $\beta^2 v_h/v_H \lesssim \varepsilon \lesssim v_h/v_H$, we require

$$\Delta \geq 2\left(\frac{v_h}{v_H}\right)^{1/2} \varepsilon^{3/2} \quad . \tag{C7}$$

In regime (3), $\varepsilon \gtrsim \frac{v_h}{v_H}$ we very roughly found

$$\Delta \gtrsim \left(\frac{v_h}{v_w}\right)^2 , \tag{C8}$$

although numerical results in this regime ought to be used. In Fig. C-1, we present several precise curves for Δ as a function of ε.

The curve in Fig. C-1 can be used to estimate the minimum rate of energy drain of a mirror machine. The warm ions will be accelerated by the ambipolar potential to an energy $\sim Mv_{es}^2/2 \sim \left(\frac{1}{2}Mv_w^2 + q\Phi\right)$ when they leave the mirror machine in a transit time $\tau_L \sim L_p/v_{es}$ (L_p is the axial scale length). The minimum power loss per unit volume is thus $P_{min} \sim n\Delta_{min}\, v_{es}^2/\tau_L v_H^2$. In principle, further improvement can be achieved because most of this energy is recoverable with direct conversion.

One practical difficulty in using warm plasma to stabilize the drift cone mode is how to have the warm plasma penetrate the ambipolar potential, especially if, the optimal warm thermal velocity, v_w, is less than v_h as is the case in regimes (1) and (2), If $v_w \sim v_h$ in regimes (1) and (2), then a much higher Δ is required; viz., $\Delta \sim (v_h/v_H)^2$ to stabilize the drift cone mode. The power loss would be a factor $(v_h/v_H)^3$ larger than in the optimum case. Possible ways to obtain a plasma with $v_w << v_h$ would be to inject the warm species as a neutral beam or with pellets.

The analysis used to determine the density of warm plasma needed for stability when $\varepsilon < \varepsilon_{cr}$ assumed a long enough wavelength so that the term in Eq. (C5) proportional to $k_\perp^2$ can be neglected. Another unstable solution to Eq. (C2) exists at shorter wavelengths with the dispersion relation given approximately as

$$(k_\perp a_H)^2 \left(\frac{m}{m} + \frac{\omega_{ci}^2}{\omega_{pi}^2}\right) - \frac{\varepsilon}{\xi} - i2\pi^{1/2}\left[\frac{v_H}{v_h} - \Delta\left(\frac{v_H}{v_w}\right)^3 + \frac{\omega_H^*}{\omega}\right] = 0 , \tag{C9}$$

where we have assumed $v_h/v_H \ll 1$ $(k_\perp a_H)^2\left(\frac{m}{M} + \frac{\omega_{ci}^2}{\omega_{pi}^2}\right) \gg \beta + \Delta\, v_H^2/v_w^2$ and

$\Delta \sim \Delta_{min}$ around optimal v_w/v_H. The solution, assuming Im $\omega \ll$ Reω, is found to be

$$\frac{\omega}{\omega_{ci}} = \frac{\varepsilon}{(k_\perp a_H)\left(\frac{m}{M} + \frac{\omega_{ci}^2}{\omega_{pi}^2}\right)} \left\{ 1 + \frac{i\varepsilon 2\pi^{1/2}\left[\frac{v_H}{v_h} - \Delta\left(\frac{v_H^3}{v_w^3}\right) + \frac{(k_\perp a_H)^2}{2}\left(\frac{m}{M} + \frac{\omega_{ci}^2}{\omega_{pi}^2}\right)\right]}{(k_\perp a_H)^4\left(\frac{m}{M} + \frac{\omega_{ci}^2}{\omega_{pi}^2}\right)^2} \right\}, \tag{C10}$$

and we see that instability exists for $(k_\perp a_H)^2 > 2\left(\Delta\, v_H^3/v_\omega^3 - \frac{v_H}{v_h}\right) \Big/ \left(\frac{m}{M} + \frac{\omega_{ci}^2}{\omega_{pi}^2}\right)$.

The maximum growth rate is found to be

$$\text{Im}\,\frac{\omega}{\omega_{ci}} = 0.45\left(\frac{v_h}{v_H}\right)^{3/2} \varepsilon^2 \Big/ \left[\left(\frac{m}{m} + \frac{\omega_{ci}^2}{\omega_{pi}^2}\right)(\Delta v_H^2 v_h/v_w^3 - 1)^3(2 + \beta)^3\right]^{1/2}.$$

In regime (1), $\Delta v_H^3/v_w^3 = v_H \exp(3/2)/v_w$; and in regime (2), $\Delta v_H^3/v_w^3 = 1.3\, v_H/v_h$.

To assess the effect of this instability, we note that it occurs for extremely short wavelengths and that it has a small growth rate compared to the real frequency. Hence, a relatively small amount of particle diffusion will stabilize these short-wavelength modes. In fact, the diffusion by the longer-wavelength modes that may be needed to establish the marginally stable states discussed earlier should suffice to stabilize the short-wavelength modes,[C5] and thus the short wavelength instability is not expected to be a factor that limits containment.

References

C1. R. F. Post and M. N. Rosenbluth, Phys. Fluids, 8 547 (1965).

C2. H. L. Berk, T. K. Fowler, L. D. Pearlstein, R. F. Post, J. D. Callen, W. C. Horton and M. N. Rosenbluth, in Proceedings Plasma Physics and Controlled Fusion Research, (IAEA, Vienna, 1965) Vol. II, p. 151.

C3. W. M. Tang, L. D. Pearlstein and H. L. Berk, Phys. Fluids, 15, 1153 (1972).

C4. H. L. Berk and L. D. Pearlstein, Phys. Fluids, 14, 1810 (1971).

C5. D. E. Baldwin, H. L. Berk and L. D. Pearlstein, in Proceedings Plasma Physics and Controlled Nuclear Fusion, (IAEA, Vienna, 1975) Vol. I, p. 301.

Fig. C-1. Plot of the minimum fraction of warm density, Δ, needed for stability as a function of $\varepsilon = a_H/R_p$ for various values of β and v_H/v_w. In these curves it is assumed $\frac{m}{M} >> (\omega_{ci}/\omega_{pi})^2$.

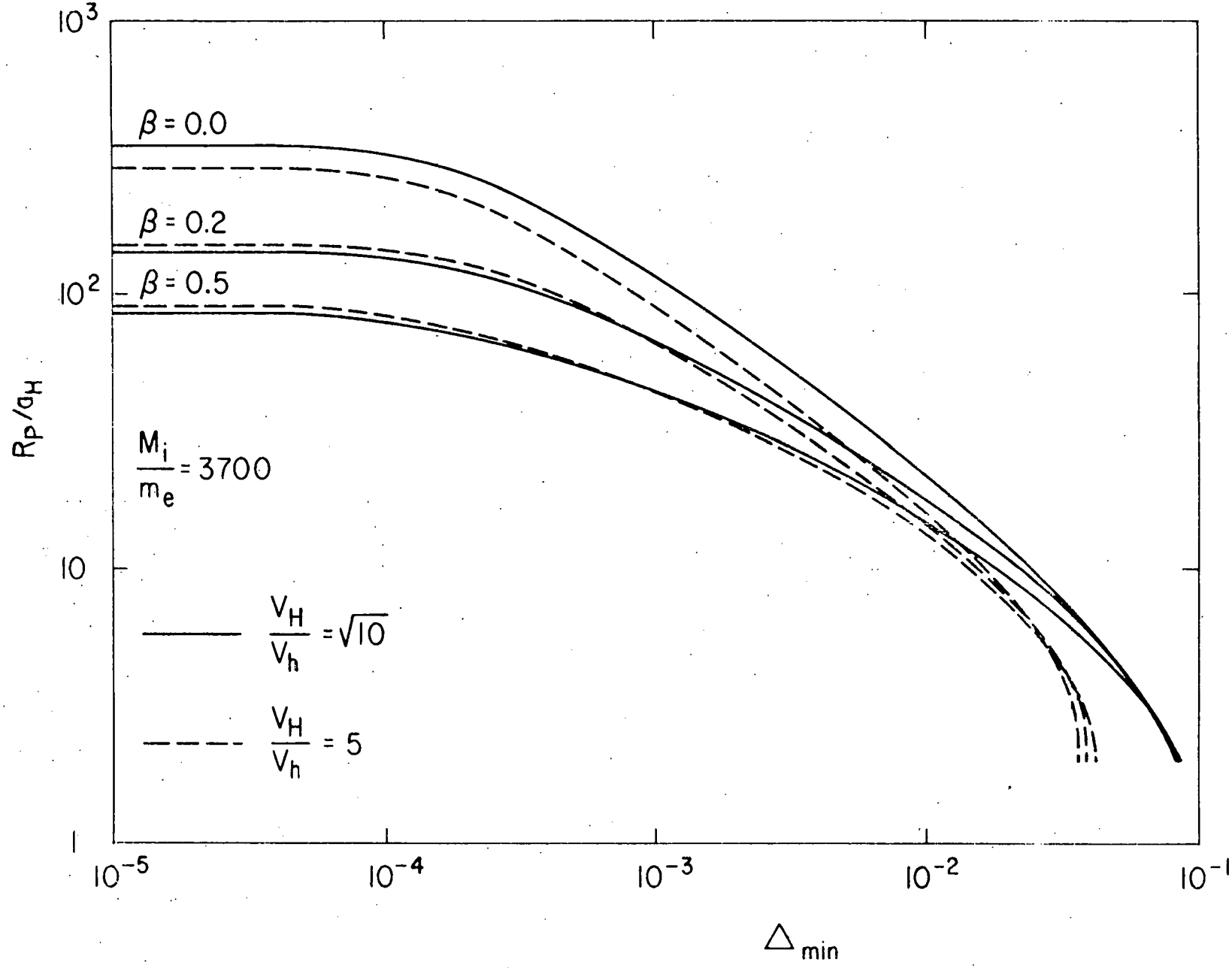
10^3
10^2
10
1
R_p/a_H
$\beta = 0.0$
$\beta = 0.2$
$\beta = 0.5$
$\frac{M_i}{m_e} = 3700$
$\frac{V_H}{V_h} = \sqrt{10}$
$\frac{V_H}{V_h} = 5$
10^{-5}
10^{-4}
10^{-3}
10^{-2}
10^{-1}
Δ_{min}

DISTRIBUTION

External:

Senior Review Panel

Dr. Robert W. Bussard
462 Santa Cecelia
Solona Beach, California 92075

Stephen O. Dean, Chairman
Division of Controlled
Thermonuclear Research
U.S. Energy Research and
Development Administration
Washington, D.C. 20545

Dr. Harold Forsen
Exxon Nuclear Co., Inc.
777-106th Avenue, NW.
Bellevue, Washington 98004

Dr. Art Fraas
Oak Ridge National Laboratory
P.O. Box Y
Oak Ridge, Tennessee 37830

Nelson J. Grace
Division of Controlled
Thermonuclear Research
U.S. Energy Research and
Development Administration
Washington, D.C. 20545

Bennett Miller
Division of Controlled
Thermonuclear Research
U.S. Energy Research and
Development Administration
Washington, D.C. 20545

Dr. Marshall N. Rosenbluth
Institute for Advanced Study
Olden Lane
Princeton, New Jersey 08540

Dr. Alvin W. Trivelpiece
Department of Physics
and Astronomy
University of Maryland
College Park, Maryland 20742

James M. Williams
Division of Controlled
Thermonuclear Research
U.S. Energy Research and
Development Administration
Washington, D.C. 20545

Special Consultants to the Panel

Dr. Solomon J. Buchsbaum
Executive Director
Research Communications Science Div.
Bell Laboratories, Craneford Corner
Holmdel, New Jersey 07733

Dr. Tihiro Ohkawa
General Atomic Company
P.O. Box 81608
San Diego, California 92138

Technical Advisors to the Panel

Dr. Richard Aamodt
Science Applications Inc.
934 Pearl Street
Boulder, Colorado 80302

Dr. Robert Conn
University of Wisconsin
Madison, Wisconsin 53706

Dr. Ronald C. Davidson
Department of Physics
and Astronomy
University of Maryland
College Park, Maryland 20742

Dr. William Ellis
Los Alamos Scientific Laboratory
P.O. Box 1663
Los Alamos, New Mexico 87545

Dr. Gareth E. Guest
General Atomic Company
P.O. Box 81608
San Diego, California 92138

Technical Advisors, con't.

Dr. Carl Henning
Division of Controlled
Thermonuclear Research
U.S. Energy Research and
Development Administration
Washington, D.C. 20545

Dr. Terry Kammash
Nuclear Engineering Dept.
University of Michigan
Ann Arbor, Michigan 48105

Dr. Gerald Kulcinski
Department of Nuclear
Engineering
University of Wisconsin
Madison, Wisconsin 53706

Dr. Norman H. Lazar
Oak Ridge National Laboratory
P.O. Box Y
Oak Ridge, Tennessee 37830

Dr. Larry M. Lidsky
Department of Nuclear
Engineering
Massachusetts Institute
of Technology
Cambridge, Massachusetts 02139

Dr. Dale Meade
Plasma Physics Laboratory
Princeton University
P.O. Box 451
Princeton, New Jersey 08540

Dr. George Miley
Nuclear Engineering Department
University of Illinois
Champagne, Illinois 61803

Dr. F. Robert Scott
Electric Power Research Inst.
3412 Hillview Avenue
P.O. Box 10412
Palo Alto, California 94303

Dr. Don Steiner
Oak Ridge National Laboratory
P.O. Box Y
Oak Ridge, Tennessee 37830

Dr. Ravindra Sudan
Laboratory of Plasma Studies
Cornell University
Ithaca, New York 14850

Dr. Keith I. Thomassen
Los Alamos Scientific Laboratory
P.O. Box 1663
Los Alamos, New Mexico 87545

United Technologies Research Center

Dr. Alan F. Haught
United Technologies Research Center
400 Main Street
East Hartford, Connecticut 06108

Dr. Russell Meyerand
United Technologies Research Center
400 Main Street
East Hartford, Connecticut 06108

SAN Operations Office

Dr. Edward Temple
San Francisco Operations Office
1333 Broadway, Wells Fargo Building
Oakland, California 94612

Dr. Robert D. Thorne
San Francisco Operations Office
1333 Broadway, Wells Fargo Building
Oakland, California 94612

DCTR Staff Coordinators

Dr. Franklin E. Coffman
Division of Controlled
Thermonuclear Research
U.S. Energy Research and
Development Administration
Washington, D.C. 20545

Dr. Milton D. Johnson
Division of Controlled
Thermonuclear Research
U.S. Energy Research and
Development Administration
Washington, D.C. 20545

DCTR, con't.

Dr. Edwin E. Kintner
Division of Controlled
Thermonuclear Research
U.S. Energy Research and
Development Administration
Washington, D.C. 20545

Dr. Oscar P. Manley
Division of Controlled
Thermonuclear Research
U.S. Energy Research and
Development Administration
Washington, D.C. 20545

PPPL

Dr. Melvin B. Gottlieb
Princeton Plasma Physics Laboratory
Princeton University
P.O. Box 451
Princeton, New Jersey 08540

Oak Ridge

Dr. John F. Clarke
Oak Ridge National Laboratory
P.O. Box Y
Oak Ridge, Tennessee 37830

LASL

Dr. Fred L. Ribe
Los Alamos Scientific Laboratory
P.O. Box 1663
Los Alamos, New Mexico 87545

Assistant Administrator for
Solar, Geothermal, and Advanced
Energy Systems

Dr. Robert L. Hirsch
Division of Controlled
Thermonuclear Research
U.S. Energy Research and
Development Administration
Washington, D.C. 20545

Internal:

D. E. Baldwin	L-388
R. E. Batzel	L-1
H. L. Berk	L-388
J. A. Byers	L-388
J. F. Clauser	L-386
F. H. Coensgen (50)	L-382
R. H. Cohen	L-388
D. L. Correll	L-387
W. F. Cummins	L-386
T. A. Cutler	L-388
T. K. Fowler (9)	L-382
C. Gormezano	L-386
M. A. Harrison	L-382
G. B. Logan	L-386
N. Maron	L-382
A. W. Molvik	L-386
M. L. Nelson	L-382
W. E. Nexsen	L-386
L. D. Pearlstein	L-388
R. F. Post	L-386
M. E. Rensink	L-388
T. D. Rognlien	L-388
T. C. Simonen	L-386
B. W. Stallard	L-386
J. J. Stewart	L-388
C. E. Taylor	L-386
W. C. Turner	L-386
D. C. Watson	L-388
CTR LIBRARY	L-387
TIC Oak Ridge (27)	
TID (15)	L-9

Printed in the United States of America
Available from
National Technical Information Service
U. S. Department of Commerce
5285 Port Royal Road
Springfield, Virginia 22151
Price: Printed Copy $___*; Microfiche $2.25

*Pages	NTIS Selling Price
1-50	$4.00
51-150	$5.45
151-325	$7.60
326-500	$10.60
501-1000	$13.60

Technical Information Department
LAWRENCE LIVERMORE LABORATORY
University of California | Livermore, California | 94550